Amplified role of potential HONO sources in O_3 formation in North China Plain during autumn haze aggravating processes

Jingwei Zhang[1**], Chaofan Lian[2,3**], Weigang Wang[2,3*], Maofa Ge[2,3,7], Yitian Guo[1,4], Haiyan Ran[1,4], Yusheng Zhang[5], Feixue Zheng[5], Xiaolong Fan[5], Chao Yan[6], Kaspar R. Daellenbach[6], Yongchun Liu[5], Markku Kulmala[5,6], Junling An[1,4,7*]

1. State Key Laboratory of Atmospheric Boundary Layer Physics and Atmospheric Chemistry (LAPC), Institute of Atmospheric Physics (IAP), Chinese Academy of Sciences, Beijing 100029, China

2. State Key Laboratory for Structural Chemistry of Unstable and Stable Species, Beijing National Laboratory for Molecular Sciences (BNLMS), CAS Research/Education Center for Excellence in Molecular Sciences, Institute of Chemistry, Chinese Academy of Sciences, Beijing 100190, China

3. School of Chemical Sciences, University of Chinese Academy of Sciences, Beijing 100049, China

4. College of Earth and Planetary Sciences, University of the Chinese Academy of Sciences, Beijing 100049, China

5. Aerosol and Haze Laboratory, Advanced Innovation Center for Soft Matter Science and Engineering, Beijing University of Chemical Technology, Beijing, 100029, China

6. Institute for Atmospheric and Earth System Research/Physics, Faculty of Science, P.O. Box 64, 00014 University of Helsinki, Helsinki, Finland

7. Center for Excellence in Urban Atmospheric Environment, Institute of Urban Environment, Chinese Academy of Sciences, Xiamen 361021, China

[*]Corresponding author: Weigang Wang (wangwg@iccas.ac.cn), Junling An (anjl@mail.iap.ac.cn)

[**]These authors contributed equally.

Abstract:

Co-occurrences of high concentrations of $PM_{2.5}$ and ozone (O_3) have been frequently observed in haze aggravating processes in the North China Plain (NCP) over the past few years. Higher O_3 concentrations in hazy days were supposed to be related to nitrous acid (HONO), but the key sources of HONO enhancing O_3 during haze aggravating processes remain unclear. We added six potential HONO sources, i.e., four ground-based (traffic, soil, and indoor emissions, and the NO_2 heterogeneous reaction on ground surface (Het_{ground})) sources, and two aerosol-related (the NO_2 heterogeneous reaction on aerosol surfaces ($Het_{aerosol}$) and nitrate photolysis ($Phot_{nitrate}$)) sources into the WRF-Chem model and designed 23 simulation scenarios to explore the unclear key sources. The results indicate that ground-based HONO sources producing HONO enhancements showed a rapid decrease with height, while the NO+OH reaction and aerosol-related HONO sources decreased slowly with height. $\mathrm{Phot}_{\mathrm{nitrate}}$ contributions to HONO concentrations enhanced with aggravated pollution levels, the enhanced HONO due to $\mathrm{Phot}_{\mathrm{nitrate}}$ in hazy days was about ten times larger than in clean days and $\mathrm{Phot}_{\mathrm{nitrate}}$ dominated daytime HONO sources (~30–70% when the ratio of the photolysis frequency of nitrate (J_{nitrate}) to gas nitric acid (J_{HNO3}) equals 30) at higher layers (>800 m). Compared with that in clean days, the $\mathrm{Phot}_{\mathrm{nitrate}}$ contribution to the enhanced daily maximum 8-h averaged (DMA8) O_3 was increased by over one magnitude during the haze aggravating process. $\mathrm{Phot}_{\mathrm{nitrate}}$ contributed only ~5% of the surface HONO in daytime with a $J_{\mathrm{nitrate}}/J_{\mathrm{HNO3}}$ ratio of 30 but contributed ~30–50% of the enhanced O_3 near the surface in NCP in hazy days. Surface O_3 was dominated by volatile organic compounds-sensitive chemistry, while O_3 at higher altitude (>800m) was dominated by NO_x-sensitive chemistry. $\mathrm{Phot}_{\mathrm{nitrate}}$ had a limited impact on nitrate concentrations (<15%) even with a $J_{\mathrm{nitrate}}/J_{\mathrm{HNO3}}$ ratio of 120. The above results suggest the potential but significant impact of $\mathrm{Phot}_{\mathrm{nitrate}}$ on O_3 formation, and that more comprehensive studies on $\mathrm{Phot}_{\mathrm{nitrate}}$ in the atmosphere are still needed.

1. Introduction

Nitrous acid (HONO) is an important source of the hydroxyl radical (OH) through its photolysis (R1), and contributes ~20–80% of the primary OH production (Alicke et al., 2002; Hendrick et al., 2014; Kim et al., 2014).

$$HONO + hv \rightarrow NO + OH \quad (R1)$$

Although it has passed forty years since the first detection of HONO in the atmosphere (Perner and Platt, 1979), the sources of HONO (especially daytime) and the dynamic parameters of HONO formation mechanisms are still not well understood (Ge et al., 2021). The current air quality models with the default gas-phase reaction (the reverse reaction of R1) always severely underestimate HONO observations, resulting in low atmospheric oxidation capacity and underestimation of secondary pollutants like ozone (O_3) (Li et al., 2010, 2011; Sarwar et al., 2008; Zhang et al., 2016, 2019a).

HONO sources can be generally classified into three categories, i.e., direct emissions, homogeneous and heterogeneous reactions. Direction emissions are mainly from traffic (Kramer et al., 2020; Kurtenbach et al., 2001; Liao et al., 2021), soil (Kubota and Asami, 1985; Oswald et al., 2013; Wu et al., 2019; Xue et al., 2021), biomass burning (Cui et al., 2021; Rondon and Sanhueza, 1989; Theys et al., 2020) and indoor combustion processes (Klosterkother et al., 2021; Liu et al., 2019; Pitts et al., 1985). The reaction of nitric oxide (NO) with OH (Pagsberg et al., 1997; Stuhl and Niki, 1972) is usually thought as the dominant homogeneous reaction and is important during daytime but could be neglected at night due to low OH concentrations, other minor homogeneous HONO sources including nucleation of NO_2, H_2O, and NH_3 (Zhang and Tao, 2010), via the photolysis of ortho-nitrophenols (Bejan et al., 2006;

Chen et al., 2021; Lee et al., 2016), via the electronically excited NO_2 and H_2O (Crowley and Carl, 1997; Dillon and Crowley, 2018; Li et al., 2008) and via $HO_2{\cdot}H_2O$+NO_2 reaction (Li et al., 2015; Li et al., 2014; Ye et al., 2015). The heterogeneous reactions mainly include nitrogen dioxide (NO_2) hydrolysis and reduction reactions on various humid surfaces (Finlayson-Pitts et al., 2003; Ge et al., 2019; Gómez Alvarez et al., 2014; Ma et al., 2013; Marion et al., 2021; Sakamaki et al., 1983; Tang et al., 2017; Yang et al., 2021b) and nitrate photolysis ($Phot_{nitrate}$) (Romer et al., 2018; Ye et al., 2016a, b; Zhou et al., 2003), and are usually thought as the main contributors to HONO concentrations in the atmosphere.

Among those potential HONO sources, the photolysis of nitrate to produce HONO in the atmosphere has received extensive attention over the past several years, and the $Phot_{nitrate}$ frequency ($J_{nitrate}$) is still argued (Gen et al.., 2022). In the laboratory studies, some researchers (Bao et al., 2018; Ye et al., 2016a, 2017) showed that $Phot_{nitrate}$ was an important HONO source, the measured $J_{nitrate}$ was 1–3 orders larger than the gas nitric acid (HNO_3) photolysis frequency (J_{HNO3}) and could reach up to 10^{-4} s^{-1}, and a number of substances including humic acid (Yang et al., 2018), sulfate (Bao et al., 2020) and TiO_2 (Xu et al., 2021) might enhance the reaction significantly; while Shi et al. (2021) found that the $J_{nitrate}/J_{HNO3}$ ratio was <10 when using suspended submicron particulate sodium and ammonium nitrate rather than $PM_{2.5}$ samples. In the field studies combining with model simulations, Kasibhatla et al. (2018) compared NO_x observations in Cape Verde Atmospheric Observatory with GEOS-Chem (Goddard Earth Observing System-Chemistry) model simulations and reported a $J_{nitrate}/J_{HNO3}$

ratio of 25–50, Romer et al. (2018) reported a $J_{nitrate}/J_{HNO3}$ ratio of < 30 based on observations of NO_x (= NO + NO_2) and HNO_3 over the Yellow Sea and a box model simulation, while larger $J_{nitrate}/J_{HNO3}$ ratios (e.g., 300) were inconsistent with the observed NO_x to HNO_3 ratios. Adopting a $J_{nitrate}/J_{HNO3}$ ratio of ~120 could greatly improve daytime surface HONO simulations (contributed ~30–40% of noontime HONO) by using the Community Multiscale Air Quality model (CMAQ) in the Pearl River Delta (Fu et al., 2019) or a box model in the Yangtze River Delta (Shi et al., 2020), while a $J_{nitrate}/J_{HNO3}$ ratio of 30 produced negligible HONO in clean periods (~2%) and slightly higher HONO in heavy haze periods (~8%) in the North China Plain (NCP) by using a box model (Xue et al., 2020) and ~1% by using CMAQ in urban Beijing (Zhang et al., 2021). Recently, Zheng et al. (2020) evaluated the effect of three $J_{nitrate}/J_{HNO3}$ ratios (1, 10 and 100) on heterogeneous sulfate formation by using CMAQ and large uncertainties of simulated sulfate concentrations were reported. The mostly adopted $J_{nitrate}/J_{HNO3}$ ratios were 1–30 or 100–120 with large uncertainties, so more efforts are needed to better understand the $Phot_{nitrate}$ impact on atmospheric oxidation capacity and concentrations of HONO and other secondary pollutants.

A number of potential HONO sources (e.g., direct emissions, NO_2 heterogeneous reactions and $Phot_{nitrate}$) have been coupled into several air quality models (An et al., 2013; Fu et al., 2019; Guo et al., 2020; Li et al., 2010, 2011; Sarwar et al., 2008; Tang et al., 2015; Xu et al., 2006; Zhang et al., 2019a, 2019b, 2020a, 2021, 2022) to improve HONO simulations. The improved HONO sources can produce more OH, which is favorable for the formation of O_3 (Fu et al., 2019; Guo et al., 2020; Li et al., 2010; Xing et al., 2019; Zhang et al., 2016, 2019a, 2022). O_3 can directly damage plants and threaten human health (Avnery et al., 2011a, b; Feng et al., 2015, 2019, 2022; Mills et al., 2007, 2018; Richards et al., 1958; Selin et al., 2009; Wilkinson et al., 2012; Zhao et al., 2021), an increasing trend of O_3 concentrations in China has been widely reported in recent years (Chen et al., 2020a; Li et al., 2020; Lu et al., 2020; Ma et al., 2016; Maji and Namdeo, 2021), and made O_3 pollution be a severe concern. A co-occurrence of high $PM_{2.5}$ and O_3 concentrations has been frequently found in China over the past few years, researchers speculated the significant role of HONO in producing O_3 enhancements (Feng et al., 2021; Fu et al., 2019; Tie et al., 2019; Yang et al., 2021a). Nevertheless, the current knowledge on the HONO difference in O_3 formation during clean and hazy days is still unclear, especially the relative contribution of each potential HONO source to O_3 enhancements during haze aggravating processes with a co-occurrence of high $PM_{2.5}$ and O_3 concentrations.

In this study, time series of pollutants including HONO, O_3, and nitrate were collected in NCP in Oct.11–31 of 2018, in which high concentrations of $PM_{2.5}$ accompanying by high O_3 concentrations were found at least twice in haze events. The specific role of each of potential HONO sources in O_3 formation will be explored during these haze events by coupling these potential HONO sources into the Weather Research and Forecasting model with Chemistry (WRF-Chem). The relative contribution of each potential HONO source to surface-averaged and vertically-averaged concentrations of HONO and O_3 will be quantified and the uncertainty in key potential HONO sources (e.g., $J_{nitrate}$) will be discussed, in order to find the key HONO sources resulting in O_3 enhancements in NCP in different pollution levels (especially during haze aggravating processes).

2. Data and methods

2.1 Observed data

The field observation was carried out during October 11–31, 2018, and the observation site was located in the west campus of Beijing University of Chemical Technology (BUCT, 116°18’37” E, 39°56’56” N) in Beijing. BUCT is an urban site close to the third ring road of Beijing, with large human activities, including vehicle emissions. Instruments were set on the 5th floor of the main teaching building. HONO was measured with a home-made water-based long-path absorption photometer (Chen et al., 2020b). A dual-channel absorption system was deployed to subtract the potential interferences, e.g., NO_2 hydrolysis. A set of on-line commercial analyzers (Thermo 48i, 42i, 49i, 43i) was used for measurements of CO, NO_x, O_3, and SO_2. To be specific, the 42i used molybdenum NO_2-to-NO converter, there would be a NO_2 overestimation for the conversion of HONO, HNO_3, or other NO_y. Considering the relatively lower concentration compared with NO_2, the impact would be minor. The chemical composition of $PM_{2.5}$ was analyzed with a Time-of-Flight Aerosol Chemical Speciation Monitor (ToF-ACSM, Aerodyne), ToF-ACSM was developed via Fröhlich et al. (2013) for Non-refractory $PM_{2.5}$ measurement. The detailed usage could be found in Liu et al. (2020), where ionization efficiency calibration of nitrate was performed using 300 nm dry NH_4NO_3 every month during the observation. An online Single Photon Ionization Time-of-Flight Mass Spectrometer (SPI-ToF-MS, Hexin) was used for the detection of a large variety of volatile organic compounds (VOCs) (Gao et al., 2013). Surface observations of O_3, NO_2, $PM_{2.5}$ and PM_{10} at 95 sites in NCP were obtained from https://quotsoft.net/air/, issued by the China Ministry of Ecology and Environment; surface meteorological observations at 284 sites in NCP were taken from the National Climatic Data Center, China Meteorological Administration (**Fig.1**).

The vertical HONO observations were not available during the Oct.11–31 of 2018 at the BUCT site, we used the observed vertical HONO concentrations from Meng et al. (2020) in urban Beijing in December of 2016 to evaluate our simulation of vertical HONO concentrations, which were also used by Zhang et al. (2021) in their CMAQ evaluation.

2.2 Model description

The improved WRF-Chem (version 3.7.1), which contained six potential HONO sources, i.e., traffic ($E_{traffic}$), soil (E_{soil}), and indoor (E_{indoor}) emissions, $Phot_{nitrate}$ in the atmosphere, and NO_2 heterogeneous reactions on aerosol ($Het_{aerosol}$) and ground (Het_{ground}) surfaces (Zhang et al., 2019a), was used in this study. $Phot_{nitrate}$ was newly added in WRF-Chem (R2) following the work of Fu et al. (2019), Ye et al. (2017), and Zhou et al. (2003):

$$pNO_3 + hv \rightarrow 0.67HONO + 0.33NO_2 \qquad \text{(R2)}$$

For $\text{Het}_{\text{aerosol}}$ and $\text{Het}_{\text{ground}}$, laboratory studies suggest that these heterogeneous reactions of NO_2 to HONO are first order in NO_2 (Aumont et al., 2003; Finlayson-Pitts et al., 2003; Saliba et al., 2000):

$$NO_2 \rightarrow HONO \quad k_a \qquad \text{(R3)}$$

$$NO_2 \rightarrow HONO \quad k_g \qquad \text{(R4)}$$

The first-order rate constants for aerosol (k_a) and ground (k_g) surface reactions are calculated below:

$$k_a = \frac{1}{4} \times v_{NO_2} \times \left(\frac{S}{V}\right) \times \gamma \qquad \text{(E1)}$$

$$k_g = \frac{f \times v_d}{H} \qquad \text{(E2)}$$

where v_{NO_2} is the mean molecular speed of NO_2, $\frac{S}{V}$ is the surface to volume ratio for aerosols, γ is the reactive uptake coefficient of aerosols, f is the proportion of deposited NO_2 reaching the surface in participating HONO formation, v_d is the dry deposition velocity of NO_2, and H is the first model layer height above the ground (~35 m). It should be noted that not 100% (50% is commonly accepted) of the participated NO_2 could be converted to HONO in R3 and R4, so k_a and k_g were multiplied by 0.5 in the final calculation of HONO heterogeneous formation via NO_2. The two factors γ and f were improved from previous studies (Li et al., 2010; Liu et al., 2014; Zhang et al., 2019a) and calculated by:

$$\gamma = 5 \times 10^{-6} \times \left(1 + \frac{SR}{\alpha}\right) \qquad \text{(E3)}$$

$$f = 0.08 \times \left(1 + \frac{SR}{\alpha}\right) \qquad \text{(E4)}$$

where SR denotes solar radiation (W m^{-2}), α is an adjusted parameter and set as 100 (W m^{-2}), thus γ and f became continuous functions during the whole day (γ and f

enhanced by ten times and reached 5×10^{-5} and 0.8 when SR reached 900 W m^{-2} at noontime, respectively).

The physical and chemical schemes used in this study are given in **Table 1**. Two domains were adopted, domain one contains 82×64 grid cells with a horizontal resolution of 81 km, domain two contains 51×51 grid cells with a horizontal resolution of 27 km (**Fig.1**), both with 17 vertical layers encompassing from the surface to 100 hPa. The observational sites are shown in the right panel of **Fig.1**, including one HONO observation site (the orange dot in urban Beijing), 95 observation sites of $PM_{2.5}$, NO_2 and O_3 (pink dots) and 284 meteorological monitoring sites (black dots).

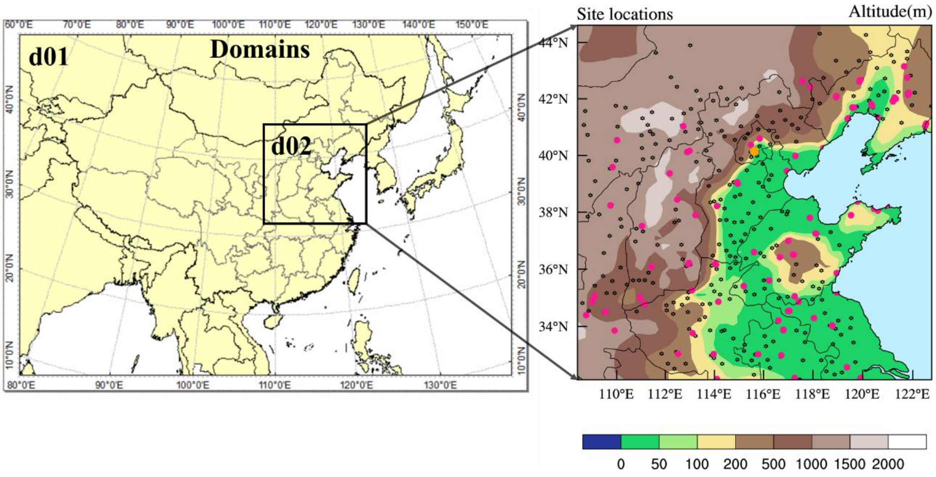

Figure 1 Domains of WRF-Chem used in this study (left panel), and the locations of one HONO observation site (the orange dot in urban Beijing), 95 environmental monitoring ($PM_{2.5}$, NO_2 and O_3) sites (deep pink dots), and 284 meteorological observation sites (black dots) in domain 2 (right panel).

The anthropogenic emissions in East Asia in 2010 were taken from the MIX emission inventory (Li et al., 2017) (http://www.meicmodel.org/), including both gaseous and aerosol species, i.e., SO_2, NO_x, CO, VOCs, NH_3, PM_{10}, $PM_{2.5}$, BC, OC and CO_2, and were provided monthly by five sectors (power, industry, residential, transportation, and agriculture) at a resolution of 0.25° × 0.25°. VOC emissions were speciated into model-ready inputs according to the MOZART chemical mechanism to build the WRF-Chem emission files. The anthropogenic emissions in China were replaced by employing the MEIC 2016 (the Multi-resolution Emission Inventory for China) developed by Tsinghua University. The NH_3 emissions in China were from Dong et al. (2010), biomass burning emissions were from Huang et al. (2012) and biogenic emissions were calculated using the Model of Emissions of Gases and Aerosols from Nature (MEGAN) (Guenther et al., 2012). Due to the sharp reduction of anthropogenic emissions in recent years, the default emission inventory was systematically overestimated in autumn of 2018, especially for SO_2 and $PM_{2.5}$ concentrations. Based on the comparison of simulations and observations (the urban Beijing site plus other 95 pollutant monitoring sites in NCP), we cut off 80% of SO_2 emissions, 50% of NH_3 emissions, 30% of toluene emissions, and 50% of $PM_{2.5}$ and PM_{10} emissions. The cut-off emissions are largely close to the emission reductions in east China during 2013 to 2017 (Zhang and Geng, 2019). The revised emissions significantly improved regional $PM_{2.5}$ simulations in NCP **(Fig.S1)**, and the simulations of gases and $PM_{2.5}$ in urban Beijing **(Fig.S2)**.

The National Centers for Environmental Prediction (NCEP) 1° × 1° final reanalysis data (FNL) (https://rda.ucar.edu/datasets/ds083.2/) were used in this study to obtain the meteorological initial and boundary conditions every 6 h. The global simulations of MOZART-4 (https://www.acom.ucar.edu/wrf-chem/mozart.shtml) were used as the chemical initial and boundary conditions (every 6 h).

Table1 Physical and chemical options in WRF-Chem used in this study

Options	WRF-Chem
Advection scheme	Runge-Kutta 3rd order
Boundary layer scheme	YSU
Cloud microphysics	Lin et al. (1983)
Cumulus parameterization	New Grell scheme
Land-surface model	Noah
Long-wave radiation	RRTM
Short-wave radiation	Goddard
Surface layer	Revised MM5 Monin-Obukhov scheme
Aerosol option	MOSAIC (Zaveri et al., 2008)
Chemistry option	Updated MOZART mechanism (Emmons et al., 2010)
Photolysis scheme	F-TUV

Totally 23 simulation scenarios were performed in this study (**Table 2**), in which the base case only considered the default homogeneous reaction (OH + NO → HONO), case 6S contained six potential HONO sources while case A, B, C, D, E and F contained each of the six potential HONO sources, respectively. Other 15 cases (A_double, A_half, …, Nit_120, D_NO_2 and D_HONO) were used to evaluate the uncertainties of the six potential HONO sources (**Table 2**). All of the cases were simulated with a spin-up of 7 days. $J_{nitrate}$ and J_{HNO3} denote the photolysis frequency of nitrate and gas nitric acid in the atmosphere, respectively. The enhancement factor for F_double was 1.25 rather than 2.0 to avoid the production rate of HONO from NO_2 reaching the surface exceeding 100%. The $0.33NO_2$ in D_NO_2 or 0.67HONO in D_HONO referred to the assumed $Phot_{nitrate}$ products in R2.

Table 2. Simulation scenarios designed in this study.

Case	HONO sources
Base	Default (OH + NO → HONO)
6S	Default + $E_{traffic}$ + E_{soil} + E_{indoor} + $Phot_{nitrate}$ ($J_{nitrate}/J_{HNO3}$ = 30) + $Het_{aerosol}$ + Het_{ground}
A	Default + $E_{traffic}$
B	Default + E_{soil}
C	Default + E_{indoor}
D	Default + $Phot_{nitrate}$ ($J_{nitrate}/J_{HNO3}$ = 30)
E	Default + $Het_{aerosol}$
F	Default + Het_{ground}
A_double	Default + 2×$E_{traffic}$
A_half	Default + 0.5×$E_{traffic}$
B_double	Default + 2×E_{soil}
B_half	Default + 0.5×E_{soil}
C_double	Default + 2×E_{indoor}
C_half	Default + 0.5×E_{indoor}
E_double	Default + $Het_{aerosol}$ (2×γ)
E_half	Default + $Het_{aerosol}$ (0.5×γ)
F_double	Default + Het_{ground} (1.25×*f*)
F_half	Default + Het_{ground} (0.5×*f*)
Nit_1	Default + $Phot_{nitrate}$ ($J_{nitrate}/J_{HNO3}$ =1)
Nit_7	Default + $Phot_{nitrate}$ ($J_{nitrate}/J_{HNO3}$ = 7)
Nit_120	Default + $Phot_{nitrate}$ ($J_{nitrate}/J_{HNO3}$ = 120)
D_NO_2	Only 0.33NO_2 produced in $Phot_{nitrate}$ for case D
D_HONO	Only 0.67HONO produced in $Phot_{nitrate}$ for case D

3.Results

3.1 Comparison of simulations and observations

3.1.1 Meteorological factors

The statistical metrics of simulated meteorological parameters at 284 sites in NCP including air temperature (T), relative humidity (RH) and wind speed (WS) were comparable with the previous modelling results of other researchers (**Table 3**). The simulated wind direction (WD) bias within 45° accounted for ~56%, and the bias within 90° accounted for ~80%, suggesting that the simulated WD captured the main observed WD.

Table 3. Performance metrics (index of agreement (IOA), RMSE (root-mean-square error) and MB (mean bias)) of WRF-Chem simulated air temperature, relative humidity, wind speed and direction at 284 meteorological sites in the North China Plain during Oct. 11–31 of 2018. The definitions of the metrics used in this study are given in **Text S1**.

	IOA	RMSE	MB	Reference
T (°C)	**0.97**	**1.4**	**-1.1**	**This work**
	0.90	2.5	0.2	(Wang et al., 2014)
	0.90	/	-0.9	(Wang et al., 2010)
	0.88	/	0.5	(Li et al., 2012)
	/	3.1	0.8	(Zhang et al., 2012)
RH (%)	**0.90**	**9.0**	**-7.1**	**This work**
	0.78	16.3	-5.5	(Wang et al., 2014)
	0.78	/	-1.3	(Wang et al., 2010)
	0.86	/	-1.1	(Li et al., 2012)
	/	17.4	-5.7	(Zhang et al., 2012)
WS (m s^{-1})	**0.48**	**1.4**	**1.3**	**This work**
	0.56	2.5	1.6	(Wang et al., 2014)
	0.65	2.1	0.9	(Wang et al., 2010)
	0.62	1.5	0.6	(Li et al., 2012)
	/	2.2	1.1	(Zhang et al., 2012)

WD Bias	*0-45°*	*45-90°*	*>90°*	
Count	*75701*	*21500*	*28075*	*135276(Total)*
Percentage	**55.96%**	**23.29%**	**20.75%**	

3.1.2 Pollutant concentrations at the BUCT site

Time series of the observational data at the BUCT site are shown in **Fig.2**, the gray shaded periods stand for three haze aggravating processes, while the cyan shaded period denotes typical clean days, respectively. The hourly largest observations of O_3 (~50–75 ppb) and $PM_{2.5}$ (~100–200 μg/m^3) were both relatively higher in hazy days than in clean days, especially for the first two haze events (the O_3 concentrations in the third haze event was relatively lower due to the higher NO_x concentrations in the urban area).

The observed $PM_{2.5}$ and nitrate trends at the BUCT site were well simulated **(Fig.2a&b)**, and NO_2 simulations generally agreed with the observations **(Fig.2c)**.

The promotion effect of the six potential HONO sources on the formation of secondary aerosols leads to an increase in concentrations of $PM_{2.5}$ and nitrate for case 6S, despite nitrate consumption through $Phot_{nitrate}$ (Li et al., 2010; Qu et al., 2019; Fu et al., 2019; Zhang et al., 2019a, 2021), detailed nitrate variation caused by each of the six potential HONO sources in case 6S is presented in **Fig.S3**. Hourly and diurnal HONO simulations at the BUCT site (**Fig.2d&3a**) were significantly improved in the 6S case (mean is 1.47 ppb) compared with the base case (mean is 0.05 ppb). The normalized mean bias (NMB) was remarkably reduced to -14.22% (6S) from -97.11% (Base), and the index of agreement (IOA) was improved significantly to 0.80 (6S) from 0.45 (Base) (**Fig.2d**). The underestimation of the simulated HONO (6S) on Oct.15 and Oct.22 was mainly caused by the earlier scavenging of pollutants at the BUCT site in the used model (**Fig.2a&d**).

As for O_3, noticeable improvements could be found at the BUCT site after considering the six potential HONO sources, especially in hazy days (**Fig.2e&f**). The mean bias (MB) was improved to -3.61 ppb (6S) from -7.09 ppb (Base), and the IOA was improved to 0.86 (6S) from 0.78 (Base) (**Fig.2e**). Specially, the 6S case significantly enhanced daytime hourly O_3 by 15–35 ppb compared with the base case and the simulated O_3 was very close to the observations in hazy days (**Fig.2e**). Larger daytime O_3 enhancements were accompanied with higher $PM_{2.5}$ concentrations during haze aggravating processes, while in clean days the daytime enhanced O_3 due to the potential HONO sources was mostly < 5 ppb (**Fig.2e&f**). The diurnal O_3 pattern during the first two haze aggravating processes is presented in **Fig.3b**, significant improvements in daily maximum 8-h (10:00–17:59) averaged (DMA8) O_3 (18.8 ppb) occurred at the BUCT site after considering the six potential HONO sources, and the NMB of DMA8 O_3 was remarkably improved to -2.38% (6S) from -47.14% (Base).

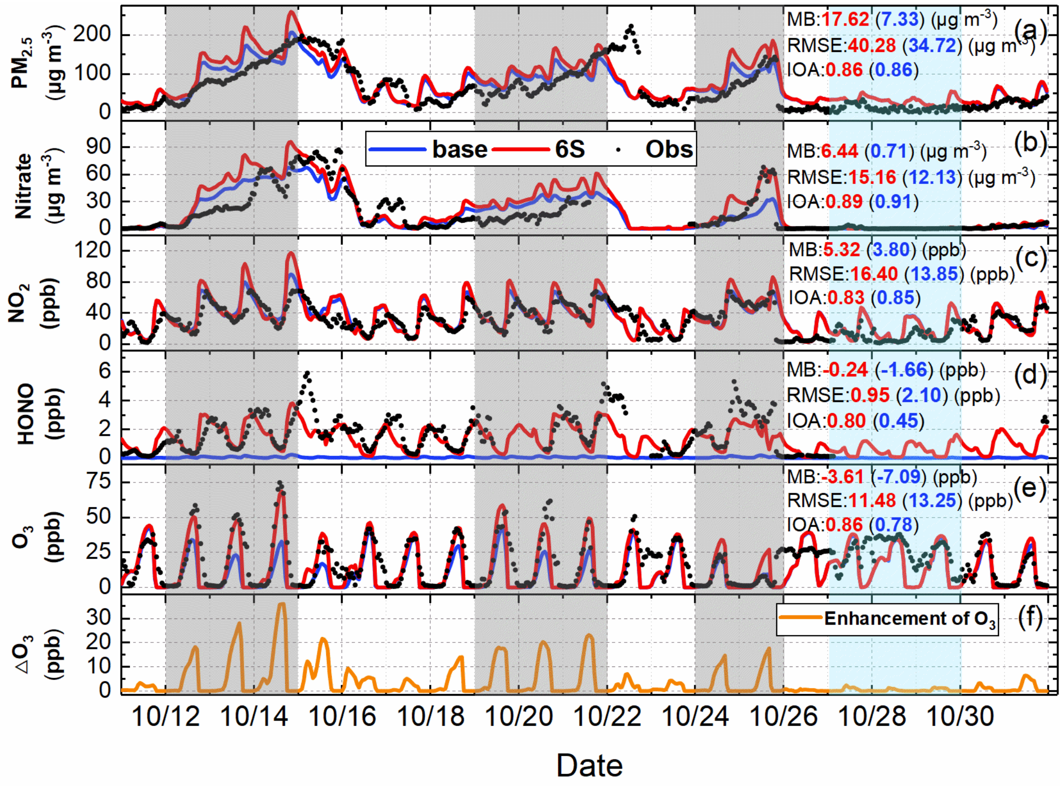

Figure 2 Comparison of simulated (Base and 6S cases) and observed hourly concentrations of $PM_{2.5}$, nitrate, NO_2, HONO and O_3 (a–e), and the hourly enhanced concentrations of O_3 ($\triangle O_3$) (f) caused by the six potential HONO sources (6S minus Base) at the BUCT site during Oct.11–31 of 2018.

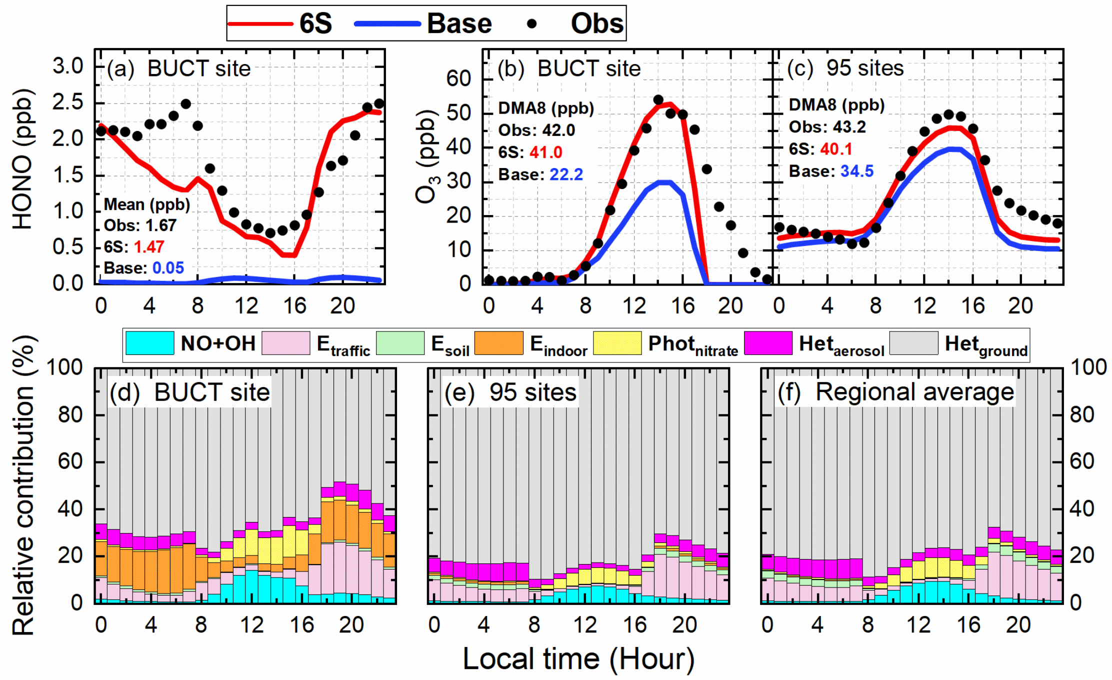

Figure 3 Comparison of diurnal mean simulations (Base and 6S cases) and observations of HONO during the study period (a) and O_3 during the first two haze events at the BUCT site (b), and O_3 averages at the 95 NCP monitoring sites during the study period (c); and the relative contributions of each of the six potential HONO sources and the reaction of OH with NO to surface HONO concentrations for the 6S case at the BUCT site (d), at the 95 monitoring sites (e) and in the whole NCP region (f) (The calculated 24-h mean HONO concentrations and DMA8 O_3 concentrations were given in panels (a) – (c)).

The relative contribution of each HONO source near the surface at the BUCT site for the 6S case is shown in **Fig.3d**. Briefly, Het_{ground} was the largest source during daytime and nighttime (~50–70%), consistent with the results of Zhang et al. (2021). $Phot_{nitrate}$ ($J_{nitrate}/J_{HNO3}$ = 30) and the NO+OH reaction contributed similarly ~1–12% during daytime. $E_{traffic}$ was important during nighttime (~10–20%) but small during daytime (<5%). The contribution of $Het_{aerosol}$ to HONO concentrations was minor

(~2–3%) in daytime and ~6–10% in nighttime. E_{soil} could be neglected while the contribution of E_{indoor} was close to that of $E_{traffic}$ in urban Beijing. The relative contribution of the potential HONO sources in this study was comparable with the result of Fu et al. (2019) by using CMAQ, except for the contribution of $Phot_{nitrate}$ due to the different $J_{nitrate}/J_{HNO3}$ ratios (30 in our study and ~120 in Fu et al. (2019)).

3.1.3 Pollutant concentrations in NCP

The 95-site-averaged hourly simulations and observations of O_3, NO_2 and $PM_{2.5}$ during the study period are shown in **Fig.4**. The six potential HONO sources significantly improved hourly O_3 simulations, remarkably enhanced the daily maximum O_3 by ~5–10 ppb during Oct. 11–25, and by ~2–4 ppb during Oct. 26–31 (**Fig.4a&b**). The simulations of NO_2 well agreed with the observations, and the mean concentrations were 22.55 (Base), 21.62 (6S) and 20.74 (Obs) ppb (**Fig.4c**). The $PM_{2.5}$ simulations generally followed the observed $PM_{2.5}$ trend but were overestimated by ~8 μg m^{-3}, with averaged concentrations of 49.94 (Base), 53.30 (6S) and 45.31 (Obs) μg m^{-3} (**Fig.4d**), respectively.

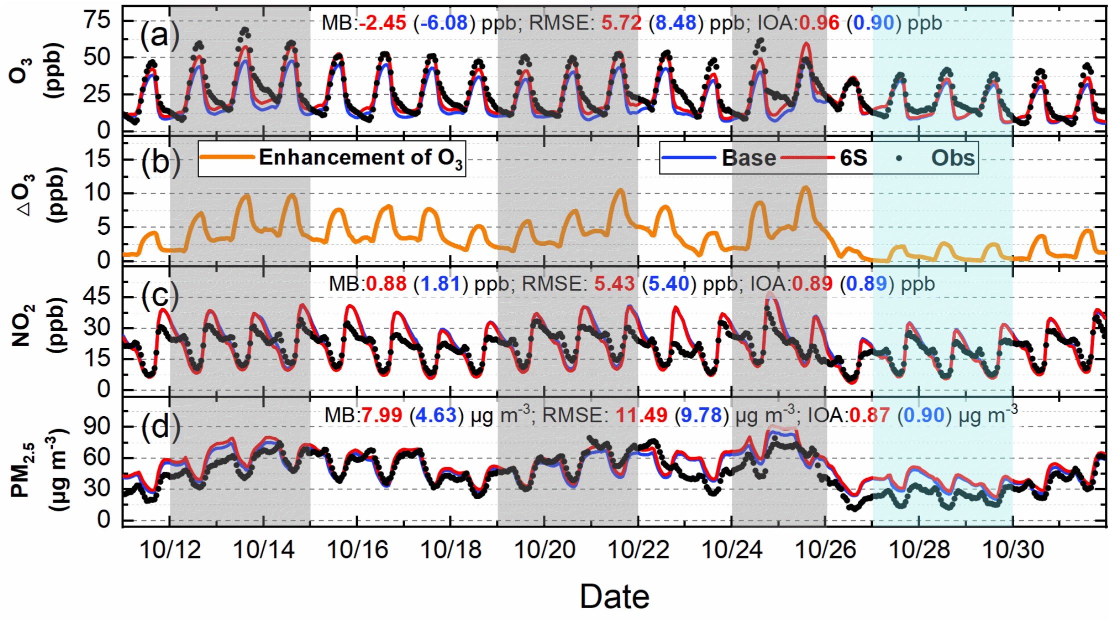

Figure 4 Comparison of 95-site-averaged hourly simulations (Base and 6S cases) and observations of O_3(a), NO_2 (c) and $PM_{2.5}$ (d), and O_3 enhancements due to the six potential HONO sources (6S minus Base case) (b) in the North China Plain during Oct.11–31 of 2018.

The 95-site-averaged diurnal simulations and observations of O_3 are presented in **Fig.3c**, O_3 simulations showed a remarkable improvement when the six potential HONO sources were considered, the six potential HONO sources produced a mean enhancement of 5.7 ppb in DMA8 O_3 and improved the NMB to -7.16% from -20.32% at the 95 sites in NCP. The 95-site-averaged diurnal simulations and observations of NO_2 and $PM_{2.5}$ during the study period are demonstrated in **Fig.S4**. NO_2 simulations generally followed the observed trend but were underestimated during 04:00 to 16:00 and overestimated after 18:00 (**Fig.S4a**), $PM_{2.5}$ simulations agreed with the observed diurnal pattern but were overestimated for both cases during the whole day (**Fig.S4b**).

The relative contribution of each HONO source near the surface at the 95 NCP sites for the 6S case is shown in **Fig.3e.** Het_{ground} was the dominant source during daytime and nighttime (~70–80%). $Phot_{nitrate}$ ($J_{nitrate}/J_{HNO3}$ = 30) and the NO+OH reaction nearly equaled and contributed ~2–8% during daytime (~5% on average). $E_{traffic}$ was important during nighttime (~10–15%) but small during daytime (<3%). The contribution of $Het_{aerosol}$ to HONO concentrations was <3% in daytime and <10% in nighttime. E_{soil} contributed ~3% in nighttime but could be neglected in daytime. The contribution of E_{indoor} was too small to be noticed at the 95 NCP sites, implying that this source was noticeable only in megacities. The relative contribution of each HONO source in the whole NCP region (all grid cells in domain two except for the seas) is presented in **Fig.3f**, the results were quite similar with those at the 95 sites (**Fig.3f**), which were representative for the whole NCP region. To further understand the role of potential HONO sources in haze aggravating processes in regional O_3 concentrations, the 95 site-averaged surface/vertical HONO concentrations and their impacts during a typical haze event (Oct. 19–21) and a clean period (Oct. 27–29) were analyzed and are shown in the following sections.

3.2 Spatial distribution of enhanced DMA8 O_3 by potential HONO sources

3.2.1 General patterns of enhanced DMA8 O_3

Fig.S5 shows surface-averaged and zonal-averaged DMA8 O_3 enhancements due to the six potential HONO sources in NCP during the study period (Oct.11-31) and three haze events (Oct.12–14, Oct.18–21 and Oct.24–25). The overall surface DMA8 O_3 enhancement decreased gradually from south (6–10 ppb) to north (2–6 ppb)

(**Fig.S5a**) and could reach 10–20 ppb under unfavorable meteorological conditions during haze events (**Fig.S5b–d**). For the first two haze events, the anti-cyclone in the Shandong peninsula carried pollutants being transported from the southeastern NCP to the western (108–112°E) and northern (39–41°N) NCP, and the six potential HONO sources led to a DMA8 O_3 enhancement of 10–20 ppb (**Fig.S5b**) and 10–15 ppb (**Fig.S5c**) in Beijing, respectively. For the third haze event, two air masses were converged to form a transport channel from south to north, the O_3 enhancement caused by the six potential HONO sources can reach 10–18 ppb in the southern NCP and decreased to 6–10 ppb in the northern NCP along the transport channel. Vertically, the DMA8 O_3 enhancements were 2–8 ppb during the whole period (**Fig.S5e**) and increased to 6–12 ppb in these haze events (**Fig.S5f–h**). The enhanced O_3 near the surface (0–100 m) was slightly smaller than that at higher altitude (**Fig.S5f–h**), due mainly to the stronger titration of O_3 by NO near the surface. The above results demonstrated that the six potential HONO sources significantly enhanced surface and vertical O_3 concentrations in NCP, especially during haze events.

3.2.2 During a typical haze aggravating process and a clean period

Fig.5 demonstrates surface-averaged and zonally-averaged DMA8 O_3 enhancements due to the six potential HONO sources in NCP during a typical haze aggravating process (Oct.19–21, 2018) and a clean period (Oct.27–29, 2018). The increasing trend of DMA8 O_3 enhancements can be clearly seen from Oct.19 to

Oct.21 near the surface and in the vertical direction. During the haze aggravating process, the surface DMA8 O_3 enhancements were ~2–10 ppb (Oct.19), ~6–12 ppb (Oct.20) and ~8–15 ppb (Oct.21), respectively; the vertical DMA8 O_3 enhancements were ~4–7 ppb (Oct.19), ~6–10 ppb (Oct.20), and ~8–15 ppb (Oct.21), respectively. While during clean days, the surface/vertical DMA8 O_3 enhancements were usually <4 ppb. The six potential HONO sources significantly enhanced surface and vertical O_3 concentrations in NCP during haze aggravating processes, the detailed role of the potential HONO sources on vertical HONO concentrations and their impacts are presented in the next section.

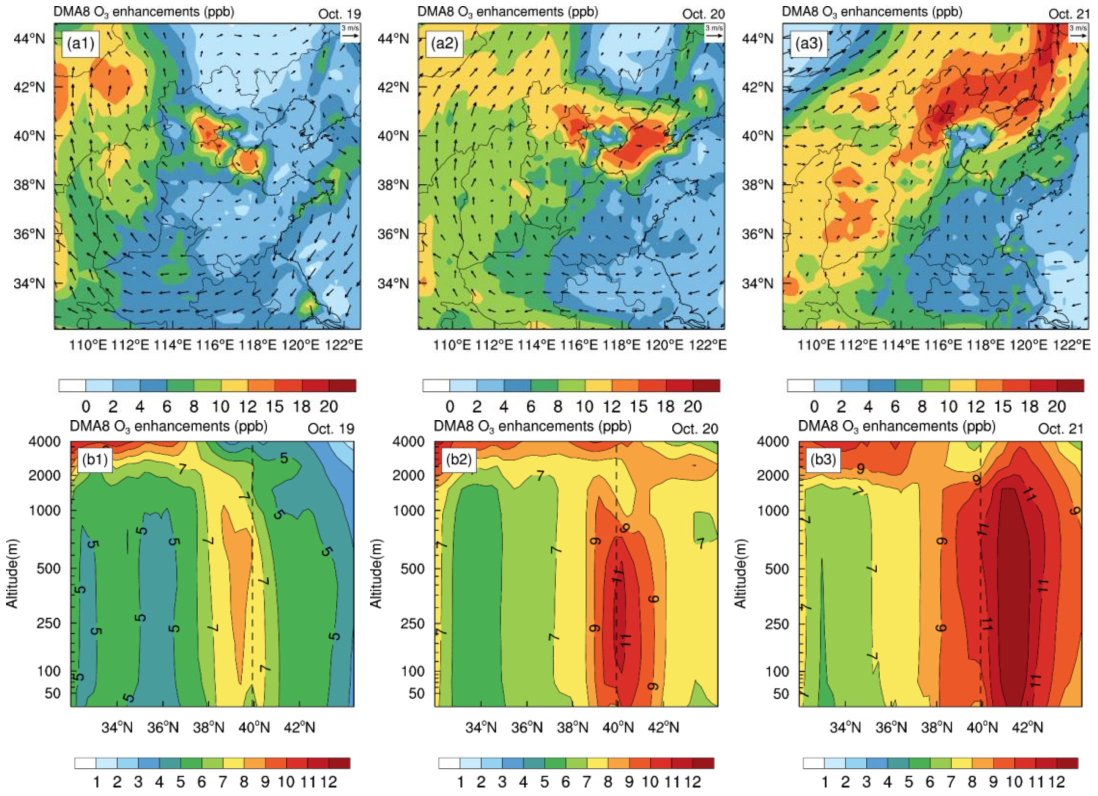

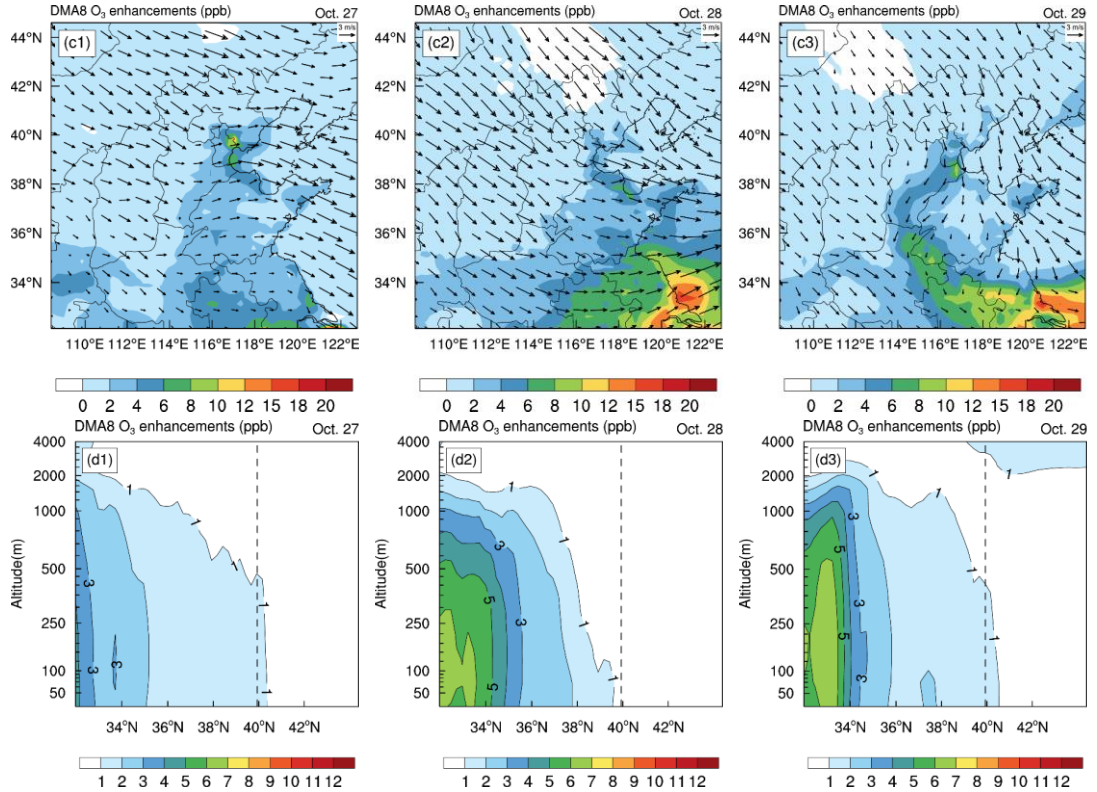

Figure 5 Surface-averaged (a1–a3, c1–c3) and zonal-averaged (b1–b3, d1–d3) DMA8 O_3 enhancements due to the six potential HONO sources in the North China Plain during a typical haze aggravating process (Oct.19–21, 2018) and a clean period (Oct.27–29, 2018) (The dashed line denotes the latitude of the BUCT site).

3.3 Vertical variations of the six potential HONO sources and their impacts

3.3.1 Six potential HONO sources and their impacts on HONO concentrations

A number of studies have conducted vertical HONO observations abroad (Kleffmann et al., 2003; Ryan et al., 2018; Sorgel et al., 2011; VandenBoer et al., 2013; Villena et al., 2011; Wang et al., 2020; Wong et al., 2011, 2012; Zhang et al., 2009) and in China (Meng et al., 2020; Wang et al., 2019; Xing et al., 2021; Zhu et al., 2011).

A decreasing trend of HONO with height was mostly observed among these studies, and our simulations also reproduced this vertical variation and were comparable with another model simulation by Zhang et al. (2021) who used CMAQ (**Fig.S6**). For a deep understanding of the role of each considered HONO source in HONO concentrations at different heights, we assessed the contributions of each potential HONO source to HONO concentrations at different heights (**Fig.6**) during Oct.11–31 of 2018.

Generally, the impacts of ground-based potential HONO sources ($E_{traffic}$, E_{soil}, E_{indoor} and Het_{ground}) on HONO concentrations decreased rapidly with height, while the NO+OH reaction and aerosol related HONO sources ($Phot_{nitrate}$ and $Het_{aerosol}$) decreased slowly with height (**Fig.6**). During daytime the NO+OH reaction, $Phot_{nitrate}$ and Het_{ground} were the three main HONO sources, while during nighttime $E_{traffic}$, $Het_{aerosol}$ and Het_{ground} were the three main contributors to HONO concentrations (**Fig.6**). The HONO concentrations via the NO+OH reaction and $Phot_{nitrate}$ were higher during daytime. The impact of E_{soil} in the NCP was small, nevertheless, Xue et al. (2021) found strong soil HONO emissions in NCP agricultural fields after fertilization, suggesting that this source may have a remarkable enhancement on regional HONO and secondary pollutants in crop growing seasons.

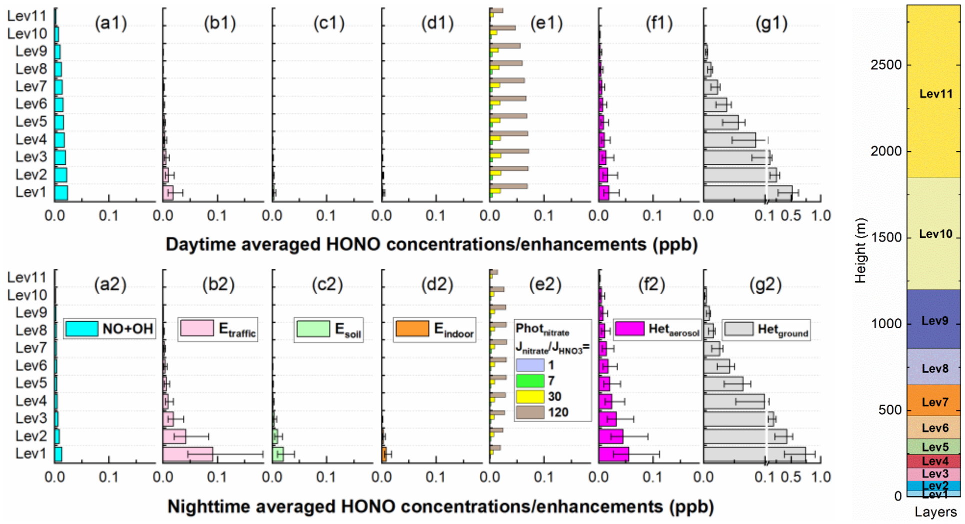

Figure 6 The 95-site-averaged daytime/nighttime HONO concentrations/enhancements at different heights when the NO+OH reaction (a1&a2) and each of the six potential HONO sources (b1–g1&b2–g2) were considered during Oct.11–31 of 2018 (The error bar denotes the uncertainties of each potential HONO source in HONO concentrations (**Table 2**). The right panel denotes the approximate height of each vertical layer above the ground).

The comparison of HONO concentrations/enhancements during a haze aggravating process and a clean period is shown in **Figs.7&8**. Generally, daytime HONO concentrations increased in haze aggravating processes and were higher than those in clean days. Het_{ground} was the dominant source of the surface HONO in both hazy and clean days and contributed 80–90% of daytime averaged HONO concentrations (**Fig.8**), however, this reaction occurred only on the ground surface, thus its relative contribution decreased with height, especially in haze aggravating processes (**Fig.8**). Although the contribution of the NO+OH reaction to daytime HONO was small near the surface, its relative contribution to HONO increased with height, especially in clean days (**Fig.8**). As for $Phot_{nitrate}$, a much larger enhancement could be found in hazy days compared with clean days. In clean days the daytime enhanced HONO by $Phot_{nitrate}$ was only 1–3 ppt in general and its contribution to daytime HONO was usually <10%, while in the haze aggravating process, the enhanced HONO concentration by $Phot_{nitrate}$ was about ten times higher than that in clean days and $Phot_{nitrate}$ became the dominant HONO source (~30–70%) at higher altitude, and both HONO concentrations and contributions by $Phot_{nitrate}$ increased with the air pollution aggravation (**Fig.7a–c, Fig.8a–c**). The contributions of direct emission sources were small and decreased when $PM_{2.5}$ increased, compared with those heterogeneous reactions. Higher concentrations of NO_2, nitrate, and $PM_{2.5}$ favored heterogeneous formation of HONO, while direct emission sources were relatively invariable under different pollution levels.

Based on our results, nitrate concentrations increased with the haze aggravating processes (**Fig.2b**), as a positive feedback effect, the elevated nitrate could in turn enhance HONO formation and further enhance the atmospheric oxidation capacity during daytime. Considering $J_{nitrate}$ was still unclear, sensitivity tests were conducted and are presented in the discussion section.

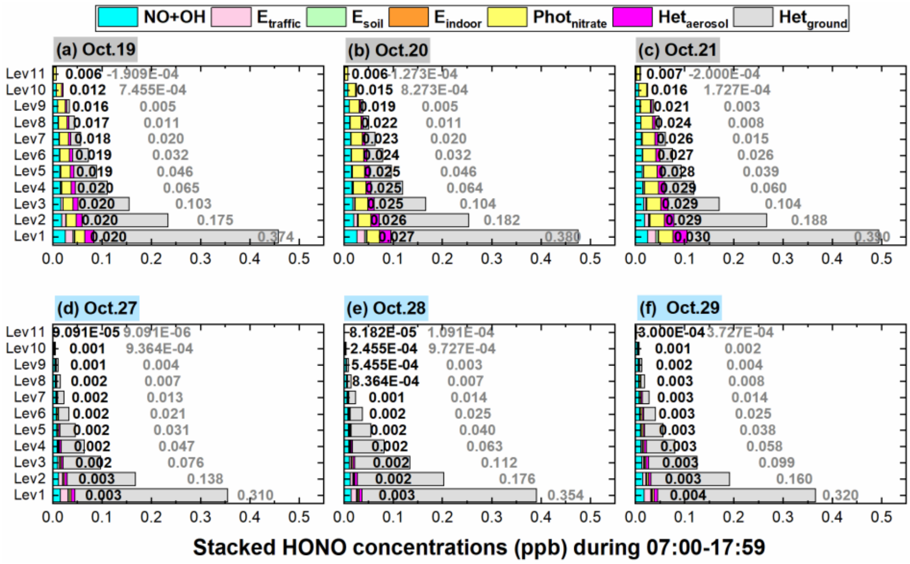

Figure 7 The 95-NCP-site-averaged daytime HONO concentrations at different heights when the NO+OH reaction and the six potential HONO sources were included during a typical haze aggravating process of Oct.19–21 (a–c) and a clean period of Oct.27–29 (d–f) of 2018 (The first column numbers in black in each graph are for $Phot_{nitrate}$, and the second column numbers in gray are for Het_{ground}).

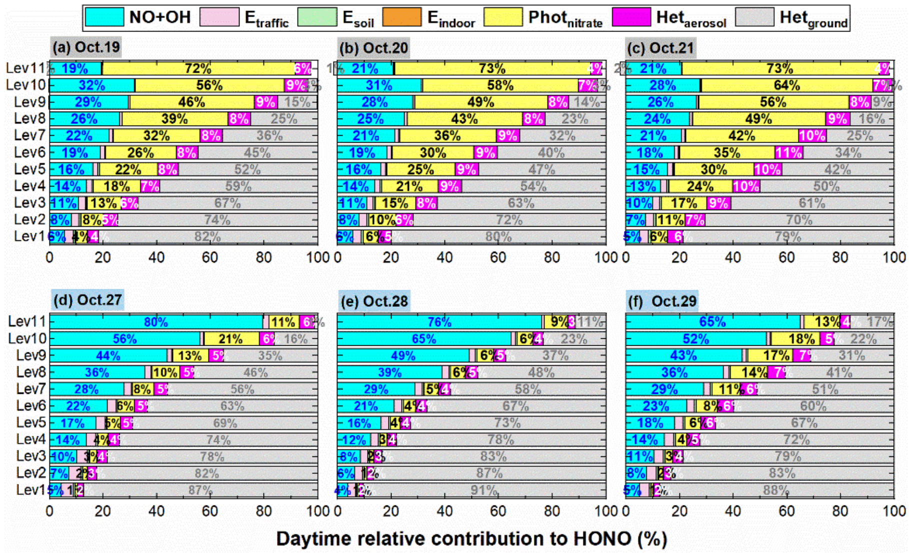

Figure 8 The 95-NCP-site-averaged relative contributions of the NO+OH reaction and each of the six potential HONO sources to daytime HONO concentrations at different heights during a typical

haze aggravating process of Oct.19–21 (a–c) and a clean period of Oct.27–29 (d–f) of 2018 (The first column numbers in blue in each graph are for the NO+OH reaction, the second column numbers in black are for $Phot_{nitrate}$, the third column numbers in white are for $Het_{aerosol}$, and the fourth column numbers in gray are for Het_{ground}).

3.3.2 Enhanced OH and its production rate

Fig.9 demonstrates daytime variations of OH production (P(OH)) and loss (L(OH)) rates near the surface and in the vertically-averaged layer (from ground to the height of 2.5km) at the 95 NCP sites for the Base and 6S cases during Oct.11–31, 2018. A significant enhancement of P/L(OH) can be found near the surface and vertically, the six potential HONO sources accelerated OH production and loss rates remarkably near the surface and noticeably in the considered vertical layers.

Near the surface, daytime P(OH) and L(OH) were significantly enhanced by~320% for the 6S case (mean was 5.27 ppb h^{-1}) compared with the base case (mean was 1.26 ppb h^{-1}). For the base case, the daytime P(OH) via the photolysis of HONO and O_3 was 0.09 ppb h^{-1} and 0.09 ppb h^{-1}, respectively, while the daytime L(OH) via the NO+OH reaction was 0.11 ppb h^{-1} and the net contribution of HONO photolysis to P(OH) was -0.02 ppb h^{-1}. After adding the six potential HONO sources in case 6S, the daytime P(OH) via the photolysis of HONO and O_3 was 1.81 ppb h^{-1} and 0.10 ppb h^{-1}, respectively, the daytime L(OH) via the NO+OH reaction was 0.48 ppb h^{-1} and the net contribution of HONO photolysis to P(OH) reached 1.33 ppb h^{-1}. HONO photolysis was the main source of the primary formation of OH, while the secondary formed OH via the reaction of HO_2+NO (3.14 ppb h^{-1}) was the dominant source of the total OH formation.

Vertically, daytime P(OH) or L(OH) was enhanced by ~105% for the 6S case (mean was 2.21 ppb h^{-1}) compared with the base case (mean was 1.08 ppb h^{-1}). For the base case, the daytime P(OH) via the photolysis of HONO and O_3 was 0.06 ppb h^{-1} and 0.10 ppb h^{-1}, respectively, while the daytime L(OH) via the NO+OH reaction was 0.07 ppb h^{-1} and the net contribution of HONO photolysis to P(OH) was -0.01 ppb h^{-1}. After coupling the six potential HONO sources in case 6S, the daytime P(OH) via the photolysis of HONO and O_3 and via the HO_2+NO reaction was 0.48 ppb h^{-1}, 0.12 ppb h^{-1} and 1.52 ppb h^{-1}, respectively, the daytime L(OH) via the NO+OH reaction was 0.15 ppb h^{-1} and the net contribution of HONO photolysis to P(OH) was 0.33 ppb h^{-1}.

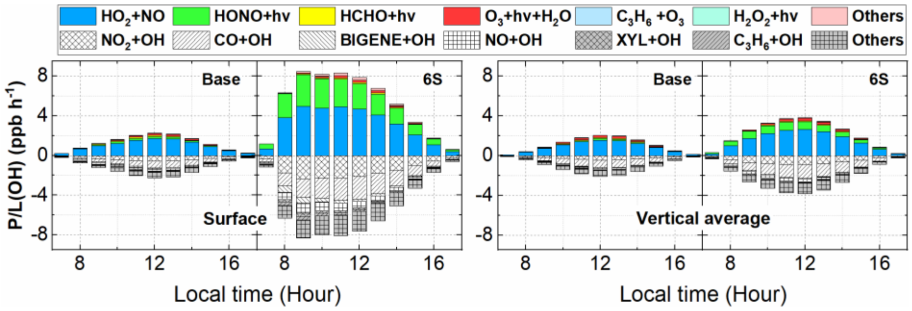

Figure 9 Diurnal mean variations of OH production (P(OH)) and loss (L(OH)) rates including major production and loss reactions near the surface and in the vertically-averaged layer (from ground to the height of 2.5km) at the 95 NCP sites for the Base and 6S cases during Oct.11–31, 2018.

Fig.10 shows the linear relationships between daytime-averaged P(OH) and $PM_{2.5}$ concentrations and between daytime-averaged OH and $PM_{2.5}$ concentrations from ground to the height of 2.5km at the 95 NCP sites during Oct. 11–31 of 2018. Both P(OH) for the two cases (Base and 6S) and the enhanced P(OH) due to the six potential HONO sources showed a strong positive correlation (r>0.8) with $PM_{2.5}$ concentrations at the 95 NCP sites, because $Het_{aerosol}$, Het_{ground} and $Phot_{nitrate}$ were significantly increased with the elevated $PM_{2.5}$. The enhanced P(OH) for the 6S case reached 0.043 ppb h^{-1} per 1μg m^{-3} of a $PM_{2.5}$ enhancement. Similarly, high positive correlation (r>0.6) could be found between OH and $PM_{2.5}$ concentrations, the OH concentrations and enhancements due to the six potential HONO sources were both higher in hazy days than those in clean days, and the enhancement of OH reached 3.62×10^4 molec cm^{-3} per μg m^{-3} of $PM_{2.5}$ for case 6S. These results were consistent with a recent field study reported by Slater et al. (2020), who found that the OH observed in haze events was elevated in central Beijing in November–December of 2016. Furthermore, two observations confirmed the key role of HONO in producing primary OH despite the relatively lower photolysis frequency in haze aggravating processes (Slater et al., 2020; Tan et al., 2018), consistent with our simulations (**Fig.S7** shows the relationship between surface $PM_{2.5}$ and photolysis frequencies of NO_2, HONO and HNO_3 in this study,).

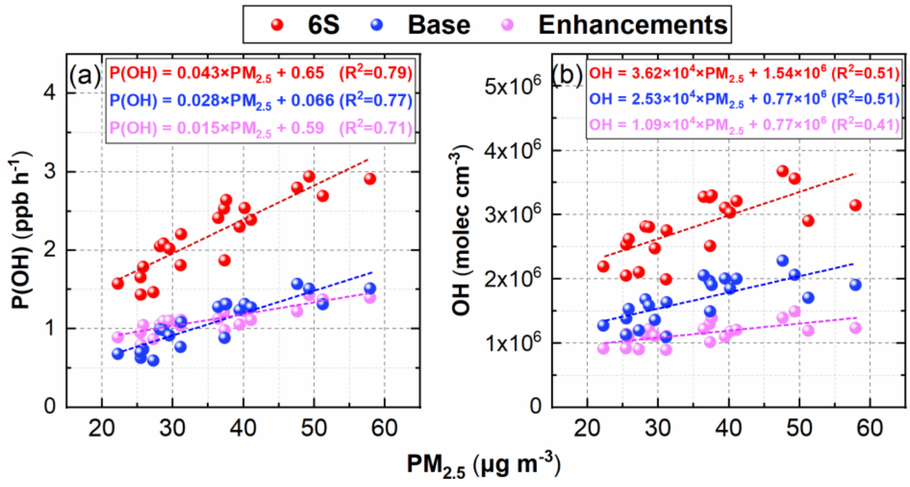

Figure 10 The linear relationships between daytime-averaged P(OH) and $PM_{2.5}$ concentrations (a) and between daytime-averaged OH and $PM_{2.5}$ concentrations (b) from ground to the height of 2.5km at the 95 NCP sites during Oct. 11–31 of 2018.

Figs.11&12 show the detailed comparisons of P(OH) and OH enhancements during a haze aggravating process and a clean period. It can be seen that both P(OH) and OH were enhanced in hazy days compared with clean days, and P(OH) and OH increased with the aggravated haze pollution. Among the six potential HONO sources, Het_{ground} was the largest contributor to the enhanced P(OH) and OH near the surface, but its contribution was relatively stable under different pollution levels and was attenuated rapidly with height in both hazy and clean days; the contribution induced by $Phot_{nitrate}$ was remarkably increased in haze aggravating processes and was about ten times higher than that in clean days; $Het_{aerosol}$ also increased with the pollution levels but with relatively small values, while the impact of other three direct emission sources of HONO was quite small.

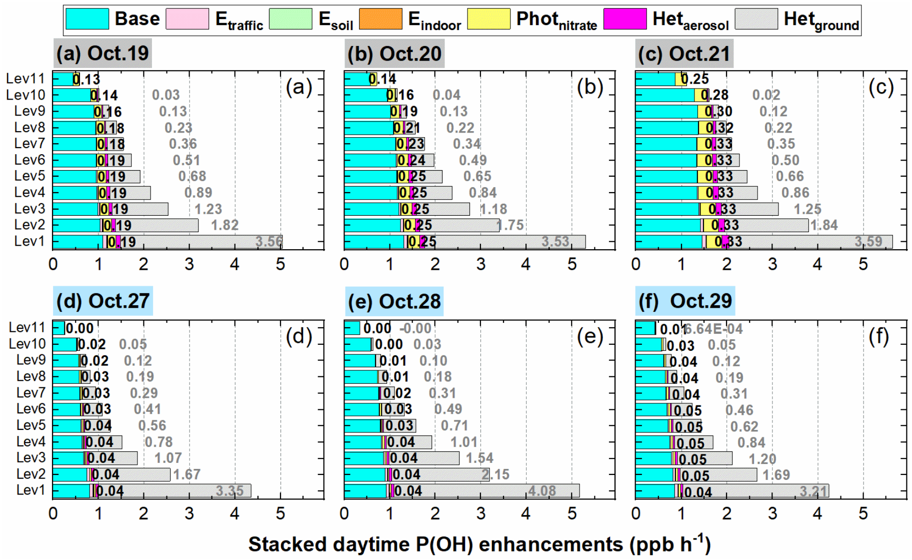

Figure 11 The 95-NCP-site-averaged daytime P(OH) for the base case and the enhancements due to the six potential HONO sources during a typical haze aggravating process of Oct.19–21 (a–c) and a clean period of Oct.27–29 (d–f) of 2018 (The first column number in black in each graph is for Phot$_{nitrate}$, and the second column number in gray is for Het$_{ground}$).

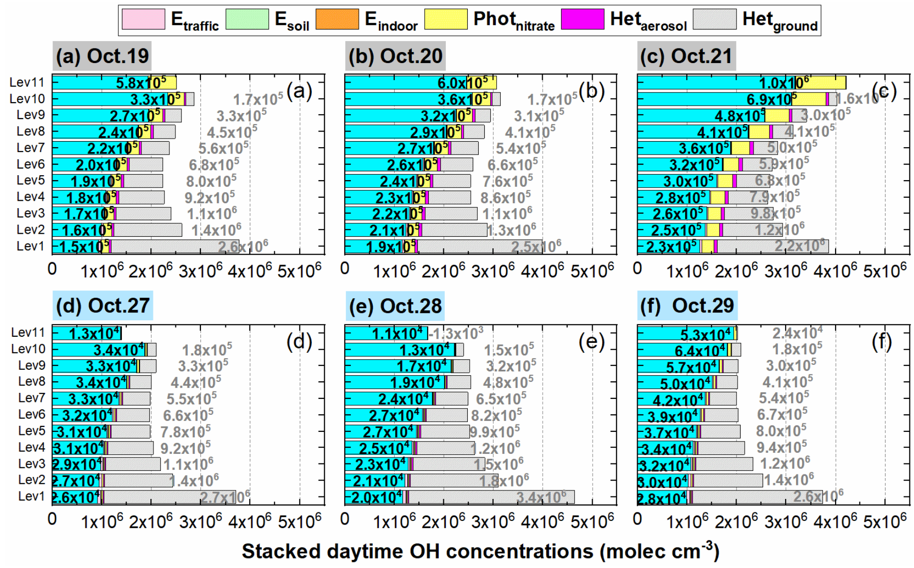

Figure 12 The 95-NCP-site-averaged daytime OH concentrations for the base case and the enhancements due to the six potential HONO sources during a typical haze aggravating process of Oct.19–21 (a–c) and a clean period of Oct.27–29 (d–f) of 2018 (The first column number in black

in each graph is for $\mathrm{Phot_{nitrate}}$, and the second column number in gray is for $\mathrm{Het_{ground}}$).

3.3.3 Enhanced DMA8 O_3

Fig.13 demonstrates the linear relationship between DMA8 O_3 enhancements and daytime $PM_{2.5}$ concentrations in each vertical layer and the averaged vertical layer for the considered eleven layers at the 95 NCP sites during Oct. 11–31 of 2018. A good correlation (r>0.8) between DMA8 O_3 enhancements and daytime $PM_{2.5}$ concentrations in the vertical averaged layer (similar reasons for the strong positive correlation between the enhanced P(OH) and $PM_{2.5}$ concentrations shown above) suggests that the enhanced O_3 due to the six potential HONO sources was larger in polluted days and increased during the haze aggravating processes. The enhanced DMA8 O_3 was < 2ppb when $PM_{2.5}$ was < 20μg m^{-3} and was >10 ppb when $PM_{2.5}$ was > 60μg m^{-3} on average, with a mean DMA8 O_3 enhancement of 0.24 ppb per μg m^{-3} of $PM_{2.5}$.

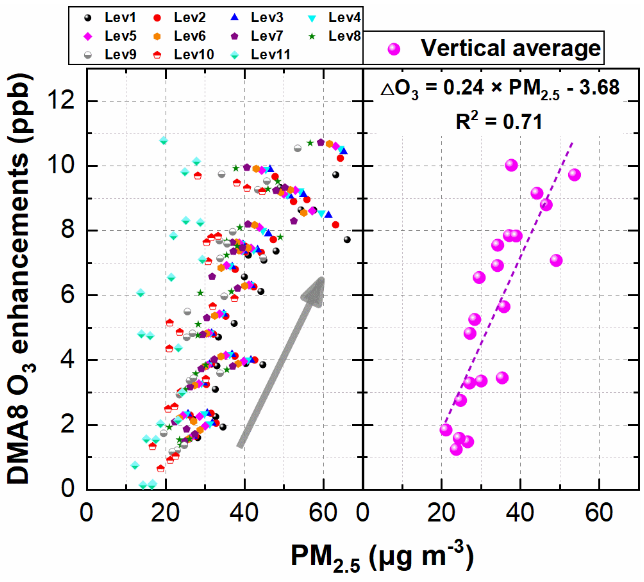

Figure 13 The linear relationship between DMA8 O_3 enhancements and daytime $PM_{2.5}$ concentrations in each vertical layer (a) and the averaged vertical layer for the considered eleven layers (b) at the 95 NCP sites during Oct. 11–31 of 2018.

Fig.14 shows the 95-NCP-site-averaged DMA8 O_3 enhancements due to the six potential HONO sources during a typical haze aggravating process of Oct.19–21 and a clean period of Oct.27–29 of 2018. A significant enhancement of DMA8 O_3 can be found during the haze aggravating process compared with during clean days. The enhanced DMA8 O_3 was ~5.5 ppb (Oct.19), ~ 7 ppb (Oct.20) and ~ 10 ppb (Oct.21), respectively, during the haze aggravating process, while that was usually ~2 ppb in clean days.

In clean days, Het_{ground} was the dominant contributor (~1.5–2 ppb) to the enhanced DMA8 O_3 among the six potential HONO sources, the contribution of $Phot_{nitrate}$ to the enhanced DMA8 O_3 was ~0.1–0.4 ppb, while that of the other four sources was minor. When it comes to the comparison between the haze aggravating process (Oct.19–21) and clean days, the DMA8 O_3 enhancements induced by Het_{ground} were doubled and reached ~3–4 ppb; the contribution of $Phot_{nitrate}$ to the enhanced DMA8 O_3 substantially increased and reached ~2–4.5 ppb (Oct.19), ~3–6 ppb (Oct.20) and ~5–10 ppb (Oct.21), respectively; $Het_{aerosol}$ showed an increasing contribution to the enhanced DMA8 O_3 during haze aggravating process (~0.3 ppb on Oct.19, ~0.4 ppb on Oct.20 and ~0.7 ppb on Oct.21), while the impacts of the other three direct emission sources ($E_{traffic}$, E_{soil}, and E_{indoor}) on the enhanced DMA8 O_3 were minor.

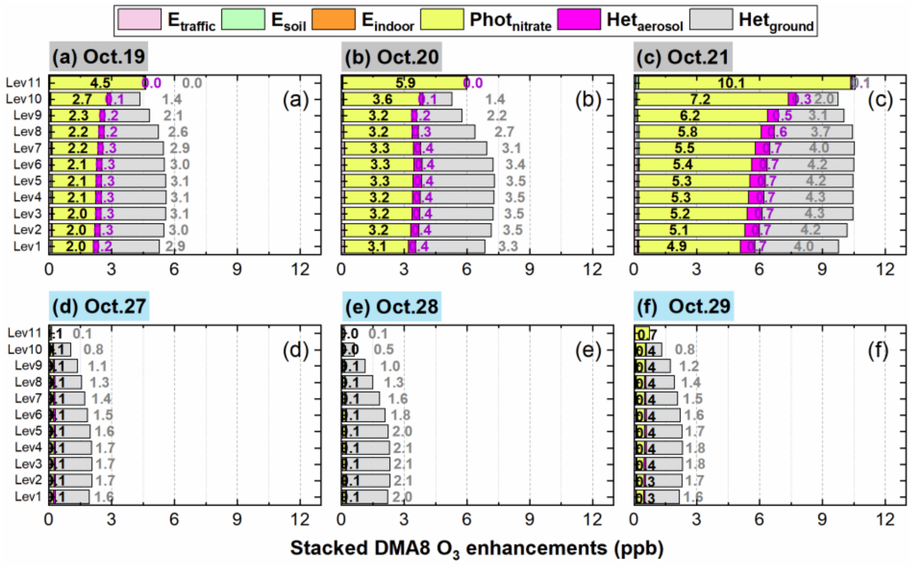

Figure 14 The 95-NCP-site-averaged DMA8 O_3 enhancements due to the six potential HONO sources during a typical haze aggravating process of Oct.19–21 (a–c) and a clean period of Oct.27–29 (d–f) of 2018 (The column in black numbers in each graph is for $Phot_{nitrate}$, the column in purple numbers in each graph is for $Het_{aerosol}$, and the column in gray numbers is for Het_{ground}).

3.4 Vertical variations of O_3-NO_x-VOCs sensitivity

Based on the results above, Phot$_{nitrate}$ could significantly enhance the DMA8 O_3 by ten times in the considered vertical layers (especially at elevated heights) in polluted events, but previous studies have not fully discussed. To better understand its role in vertical O_3 formation, the O_3-NO_x-VOCs sensitivity was analyzed by using the $P(H_2O_2)/P(HNO_3)$ ratio proposed by Sillman (1995), which is more suitable than the concentration ratio of H_2O_2/HNO_3 because of the large dry deposition velocity of the two gases in the troposphere (Sillman, 1995). A transition point of $P(H_2O_2)/P(HNO_3) = 0.35$ was suggested by Sillman (1995), when $P(H_2O_2)/P(HNO_3)$ was <0.35, O_3 shows VOCs-sensitive chemistry (increasing VOC concentrations can significantly elevate O_3 levels) and when $P(H_2O_2)/P(HNO_3)$ was >0.35, O_3 tends to NO_x-sensitive chemistry (increasing NO_x concentrations can significantly elevate O_3 levels).

Fig.15 demonstrates the 95-NCP-site-averaged $P(H_2O_2)/P(HNO_3)$ ratio at each vertical layer for the 6S case during a typical haze aggravating process of Oct.19–21 and a clean period of Oct.27–29 of 2018. Obviously opposite O_3 sensitivity appeared between the lower layers (VOCs sensitive) and the higher layers (NO_x sensitive) in both clean and hazy days, and the transition point usually appeared at the eighth layer (~600–800 m).

The Phot$_{nitrate}$ reaction is assumed to produce HONO and NO_x (Zhou et al., 2003; Romer et al., 2018; Gen et al., 2022), this reaction not only enhances OH concentrations via HONO photolysis, but also directly releases NO_x back into the troposphere. Considering the NO_x-sensitive O_3 chemistry at higher layers (>800m), elevating OH and NO_x concentrations are both favorable for O_3 formation, especially in haze aggravating processes with abundant nitrate (detailed vertically enhanced O_3 production/loss rates induced by $Phot_{nitrate}$ are shown in **Fig.S8**).

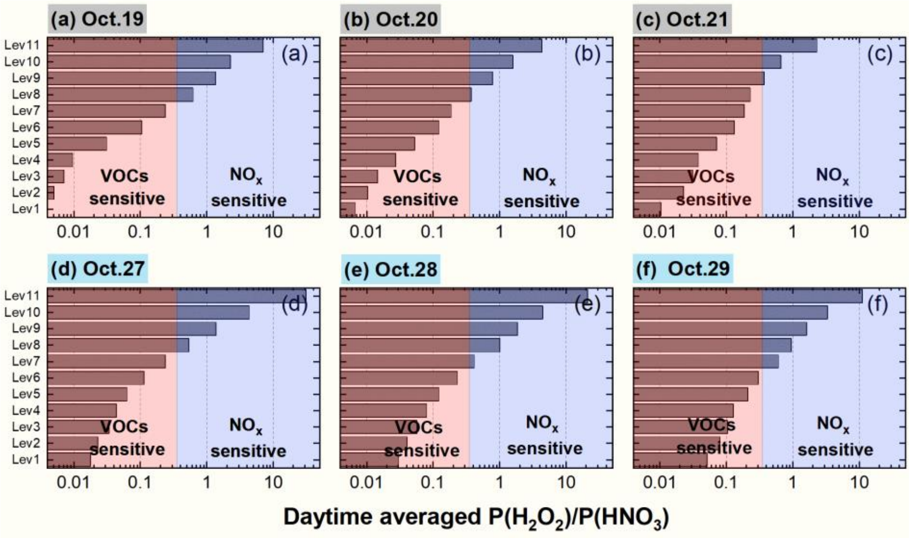

Figure 15 The 95-NCP-site-averaged $P(H_2O_2)/P(HNO_3)$ ratio at each vertical layer for the 6S case during a typical haze aggravating process of Oct.19–21 (a–c) and a clean period of Oct.27–29 (d–f) of 2018.

The specific role of the produced HONO or NO_2 via the $Phot_{nitrate}$ reaction (R2) in DMA8 O_3 enhancements was further analyzed and is shown in **Fig. 16**, the produced NO_2 and HONO jointly promoted O_3 formation and increased DMA8 O_3 concentrations. From the surface to ~1200m (Level 9), the DMA8 O_3 enhancements for case D_HONO was ~5 times those for case D_NO_2, while at ~2000 m (Level 11) the DMA8 O_3 enhancements for case D_HONO was ~2 times those for case D_NO_2. A balance exists between the propagation of the free radical interconversion cycle and the rate of termination of the cycle for the O_3 formation chemistry (Gligorovski et al., 2015), considering the 0.67 and 0.33 yields (ratio is 2) for the two products, we could conclude that the impact of produced HONO on O_3 enhancements was larger than that of produced NO_2 near the surface, while at higher altitude (>2000 m) the impacts of the two products were similar.

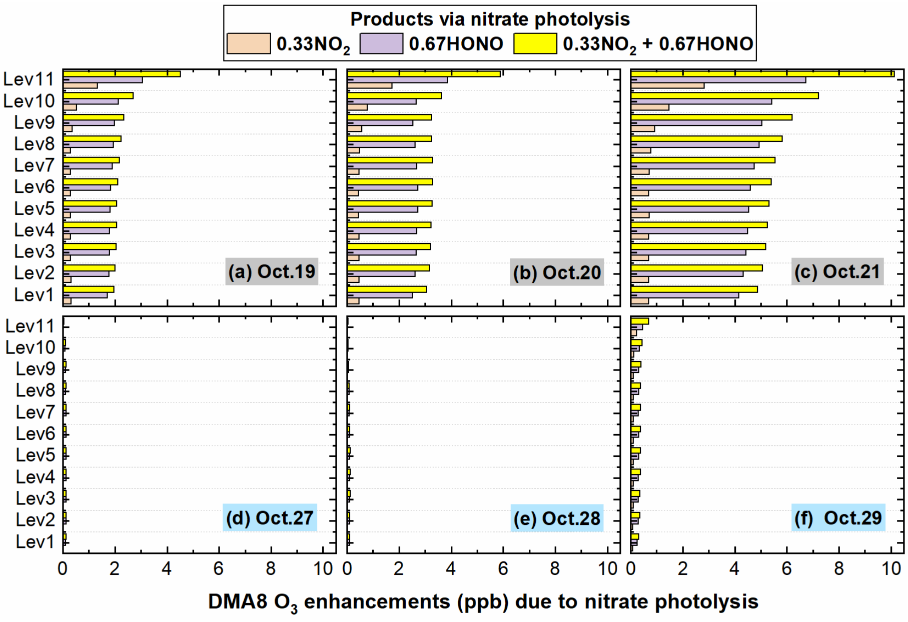

Figure 16 The 95-NCP-site-averaged DMA8 O_3 enhancements due to nitrate photolysis with three product scenarios (cases D_NO_2, D_HONO and D) during a typical haze aggravating process of Oct.19–21 (a–c) and a clean period of Oct.27–29 (d–f) in 2018.

4. Discussion

4.1 Vertical variations of potential HONO sources

The relative contribution of potential HONO sources near the surface, corresponding to the first model layer (0 to ~35 m) in our simulation, was quantified in previous modelling studies (Fu et al., 2019; Xue et al., 2020; Zhang et al., 2021), however, for those potential HONO sources, their relative contributions to HONO concentrations near and above the surface should be different. Based on our results (**Figs.7&8**), the effects of aerosol related HONO sources would be severely underestimated in hazy days when only focused surface HONO, especially for $\mathrm{Phot_{nitrate}}$. Near the surface in NCP, the daytime contribution of $\mathrm{Phot_{nitrate}}$ to HONO concentrations in hazy days was only ~4–6%, but this source contributed ~35–50% of the enhanced DMA8 O_3 (**Fig.14a–c**); above the eighth layer (~800 m), this source contributed ~50–70% of HONO concentrations and ~50–95% of the enhanced DMA8 O_3 (**Fig.14a–c**).

A recent observation in urban Beijing reported vertical HONO concentrations from three heights above the ground and found that extremely high HONO concentrations occurred at 120 m (~5 ppb) and 240 m (~3 ppb) rather than near the surface (~1.2 ppb) during 12:00 in a typical hazy day (Zhang et al., 2020b). The observation was unusual at noontime under strong convection conditions, inconsistent with those most previous observations indicating a HONO decrease trend with height, especially with the observational results of Zhu et al. (2011) and Meng et al. (2020) and simulated results of Zhang et al. (2021) and ours in **Fig.S6** at the same observational site. The contributions of different HONO sources at each layer were analyzed by using a box model, but ~80–90% of the noontime HONO at higher layers could not be explained by the known HONO formation mechanisms (Zhang et al., 2019c). The box model neglected the vertical convection, so the ground related

HONO sources had no contribution to HONO concentrations at the higher layers, thus their HONO simulations were actually underestimated compared with our results and the previous studies of Wong et al. (2011) and Zhang et al. (2021).

4.2 Uncertainties of $J_{nitrate}/J_{HNO3}$ ratios and their impacts

4.2.1 Uncertainties of $J_{nitrate}/J_{HNO3}$ ratios in DMA8 O_3 enhancements

Based on our results, Het_{ground} and $Phot_{nitrate}$ were the two major contributors to the enhanced DMA8 O_3, especially for $Phot_{nitrate}$ in hazy days with higher $PM_{2.5}$ concentrations. The uncertainties of $Phot_{nitrate}$ (four $J_{nitrate}/J_{HNO3}$ ratios) in O_3 enhancements were analyzed and are shown in **Fig.17** (The uncertainties of Het_{ground} are presented in **text S2**). During the haze aggravating process, the enhanced DMA8 O_3 near the surface increased from ~0.3 to ~0.5 ppb, from ~0.9 to ~2 ppb, from ~2 to ~6 ppb, and from ~5 to ~12 ppb, with the $J_{nitrate}/J_{HNO3}$ ratio being 1, 7, 30, 120, respectively, and the enhanced O_3 increased with altitude. In clean days, the impact of $Phot_{nitrate}$ on O_3 enhancements was small (<1 ppb) even with a $J_{nitrate}/J_{HNO3}$ ratio of 120.

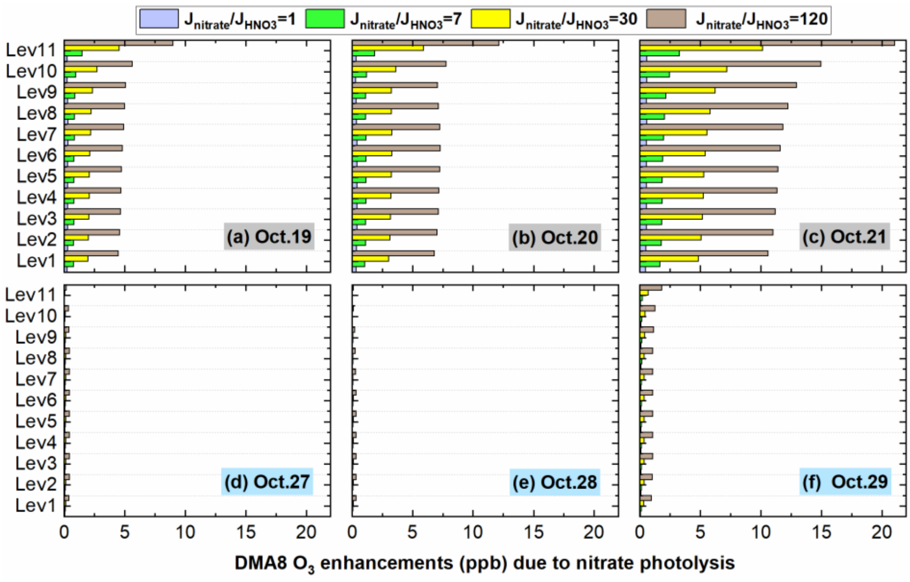

Figure 17 The 95-NCP-site-averaged DMA8 O_3 enhancement induced by nitrate photolysis with four $J_{nitrate}/J_{HNO3}$ ratios (1, 7, 30 and 120) during a typical haze aggravating process of Oct.19–21 (a–c) and a clean period of Oct.27–29 (d–f) of 2018.

4.2.2 Uncertainties of $J_{nitrate}/J_{HNO3}$ ratios in nitrate concentrations

We found considerable enhancements in O_3 concentrations induced by $Phot_{nitrate}$, yet it is still unclear that to what extent $Phot_{nitrate}$ could influence nitrate concentrations. The overall nitrate concentrations for the base case and the nitrate enhancements induced by the potential HONO sources decreased with rising altitude except for $Phot_{nitrate}$ (**Fig.S9a**). Het_{ground} enhanced nitrate concentrations by ~1.5 μg m^{-3} near the surface and the enhancements decreased to < 0.5μg m^{-3} above the eighth model layer (~800m); the nitrate enhancements due to $Het_{aerosol}$ and $E_{traffic}$ near the surface were ~0.2 and ~0.1 μg m^{-3}, respectively, and were < 0.1 and < 0.04 μg m^{-3} above the sixth model layer (~500m). For $Phot_{nitrate}$, the overall impact of four

$J_{nitrate}/J_{HNO3}$ ratios on nitrate concentrations is shown in **Fig.S9b**, a smaller $J_{nitrate}/J_{HNO3}$ ratio of 1 or 7 had a limited impact on nitrate concentrations of ~0–0.05 μg m^{-3}, a $J_{nitrate}/J_{HNO3}$ ratio of 30 slightly decreased nitrate concentrations by ~0.2 μg m^{-3}, while the $J_{nitrate}/J_{HNO3}$ ratio of 120 decreased vertical nitrate concentrations by ~0.3–0.8 μg m^{-3}. The relative nitrate changes caused by $Phot_{nitrate}$ were calculated by the differences between four cases added $Phot_{nitrate}$ (cases Nit_1, Nit_7, D and Nit_120) and the base case (**Fig.S9c**). The vertical nitrate concentrations were reduced by ~0–0.4% ($J_{nitrate}/J_{HNO3}$=1), ~0–2% (7), ~2–5% (30) and ~10–14% (120) at the 95 NCP sites, meaning that the $Phot_{nitrate}$ impact on vertical nitrate concentrations is limited (<5%) when adopting a relatively small $J_{nitrate}/J_{HNO3}$ ratio (< 30) (**Fig.S9c**).

Romer et al. (2018) found a $J_{nitrate}/J_{HNO3}$ ratio of 10 or 30 had a much larger effect on HONO than on HNO_3, and $Phot_{nitrate}$ accounted for an average of 40% of the total production of HONO, and only 10% of HNO_3 loss with a $J_{nitrate}/J_{HNO3}$ ratio of 10 (Fig.5 in Romer et al. (2018)), consistent with our study. From the production rate of gas HNO_3 (P_{HNO3}) in **Fig.S10**, we can find that an increase in the $J_{nitrate}/J_{HNO3}$ ratio for $Phot_{nitrate}$ simultaneously enhances the HNO_3 production rate, and is favorable for nitrate formation via the reaction between HNO_3 and NH_3. Nitrate consumption is mitigated by the faster nitrate formation, this is the main reason for less perturbation of the nitrate budget influenced by $Phot_{nitrate}$.

Fig.18 shows the detailed relative changes of nitrate caused by $Phot_{nitrate}$ during a typical haze aggravating process and a clean period (corresponding concentrations are shown in **Fig.S11**). The percentage nitrate reduction was usually smaller in hazy days than in clean days, mainly due to the slightly weaker photolysis frequency in pollution events (**Fig.S7**). The nitrate reduction was <5% when adopting a $J_{nitrate}/J_{HNO3}$ ratio of 30 in both clean and hazy days and was <15% in most cases even when the $J_{nitrate}/J_{HNO3}$ ratio reached 120.

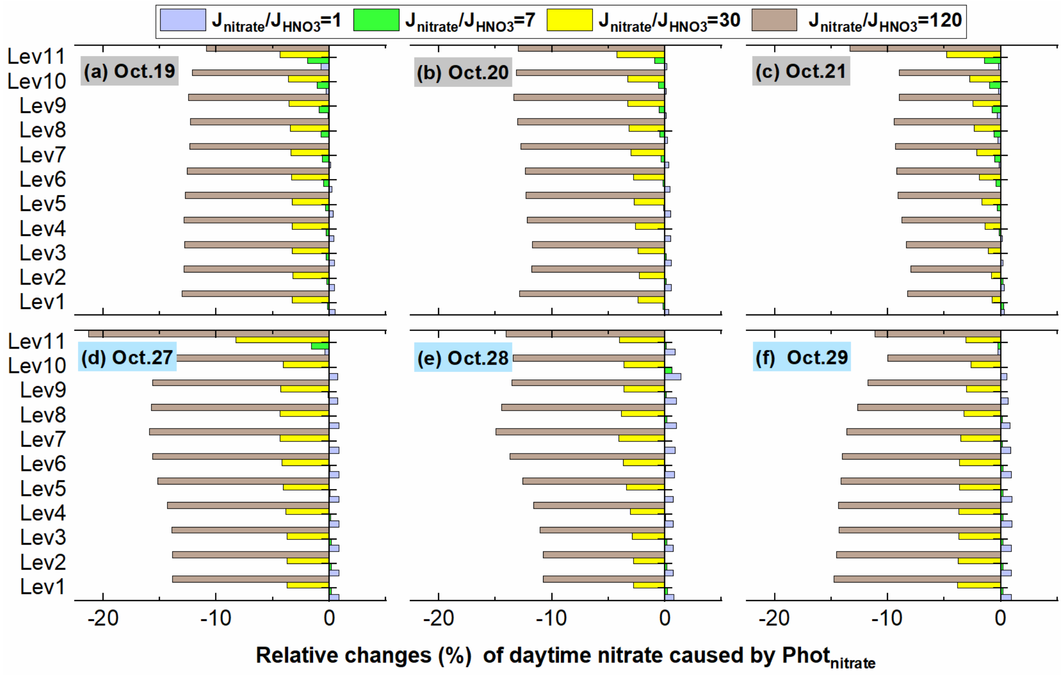

Figure 18 The 95-NCP-site-averaged relative changes of nitrate with four $J_{nitrate}/J_{HNO3}$ ratios (1, 7, 30 and 120) compared with the base case during a typical haze aggravating process of Oct.19–21 (a–c) and a clean period of Oct.27–29 (d–f) of 2018.

4.2.3 Possible ranges of the $J_{nitrate}/J_{HNO3}$ ratio

From the above discussion, we can find that the enhanced OH and O_3 due to $Phot_{nitrate}$ are remarkable during haze aggravating processes, and the exact value of the $J_{nitrate}/J_{HNO3}$ ratio requires more studies.

Fig. 19 shows diurnal patterns of surface-averaged and vertically-averaged simulations of the $Phot_{nitrate}$ frequency with four different $J_{nitrate}/J_{HNO3}$ ratios at the 95 NCP sites during the study period. The $Phot_{nitrate}$ frequency at 12:00 was 3.7×10^{-7}, 2.6×10^{-6}, 1.1×10^{-5} and 4.5×10^{-5} s^{-1}, when adopting a $J_{nitrate}/J_{HNO3}$ ratio of 1, 7, 30 and 120, respectively. The corresponding vertically-averaged $Phot_{nitrate}$ frequency was slightly larger (~10%) and was 4.2×10^{-7}, 2.9×10^{-6}, 1.3×10^{-5} and 5.0×10^{-5} s^{-1}, respectively. Adopting a $J_{nitrate}/J_{HNO3}$ ratio of 30 in the 6S case, with the corresponding $J_{nitrate}$ of 1.1–1.3×10^{-5} s^{-1}, produced ~30–50% of the enhanced O_3 near the surface in hazy days (**Fig.13**), and ~70–90% of the enhanced O_3 at higher layers (>800 m).

The reported values of $J_{nitrate}$ from previous studies are summarized in **Table 4**. The experimental $J_{nitrate}$ values have been controversial over the past two decades and are still arguable currently. In our simulations for the 6S case, $Phot_{nitrate}$ contributed from ~1% (clean days) to ~5% (hazy days) to surface HONO during daytime when using the $J_{nitrate}/J_{HNO3}$ ratio of 30 in NCP, consistent with <8% at a rural site in NCP reported by Xue et al. (2020) and ~1% at urban Beijing reported by Zhang et al. (2021) using the same ratio; however, the increasing contribution of $Phot_{nitrate}$ to HONO concentrations with rising altitude based on our simulations (**Fig.7**), has not been discussed in previous research. Furthermore, we found that the overall $Phot_{nitrate}$ impact to OH and O_3 would be severely underestimated when the $Phot_{nitrate}$ contribution to vertical HONO was excluded.

A larger $J_{nitrate}/J_{HNO3}$ ratio of 120 for $Phot_{nitrate}$ (4.5–5.0×10^{-5} s^{-1} at 12:00) produced ~25–30% of noontime HONO in NCP in our study (**Fig.S12**), comparable with 30–40%

in previous modelling studies (Fu et al., 2019; Shi et al., 2020) when using the $J_{nitrate}/J_{HNO3}$ ratio of 118.57 ($8.3\times10^{-5}/\ 7\times10^{-7}$). In haze aggravating processes, the contribution of $Phot_{nitrate}$ ($J_{nitrate}/J_{HNO3}$ = 120) to the DMA8 O_3 enhancements reached ~5–10 ppb near the surface and ~8–20 ppb above the tenth model layer (**Fig.17**), these enhancements were extremely large. In a previous modelling study by Fu et al. (2020), the daytime surface O_3 simulations were systematically overestimated by ~ 5 ppb in NCP in winter (**Fig.S4** in Fu et al. (2020)), the inclusion of $Phot_{nitrate}$ ($J_{nitrate}/J_{HNO3}$ = 118.57) in their study might cause the overestimation. From the above, a $J_{nitrate}/J_{HNO3}$ ratio of 120, or a $J_{nitrate}$ value of ~4–5×10^{-5} s^{-1} is possibly overestimated. When adopting the maximum $J_{nitrate}$ value of 10^{-4} s^{-1} reported by Ye et al. (2016a) and Bao et al. (2018), we reasonably speculate that O_3 simulations will be significantly overestimated, especially at higher altitude with NO_x-sensitive O_3 chemistry (**Fig.15**).

Romer et al. (2018) and Kasibhatla et al. (2018) suggested that a $J_{nitrate}/J_{HNO3}$ ratio of 30 or smaller would be more suitable, being about the minimum value reported by Ye et al. (2016a) and Bao et al. (2018), this ratio has shown significant influence on the O_3 simulations in haze aggravating processes in this study. The lack of photo-catalyzer in suspended submicron particulate sodium and ammonium nitrate may cause a lower $J_{nitrate}/J_{HNO3}$ ratio (<10) reported by Shi et al. (2021), so more chamber experiments need to be conducted by using the particles collected in the real atmosphere. Choosing a larger $J_{nitrate}$ value might cover up other ground-based unknown HONO sources, creating an illusion of good model simulations of daytime HONO, but resulting in overestimation of O_3 concentrations. Considering the uncertainties of NO_x or VOCs emissions, which also significantly impact O_3 simulations, more studies are needed to find the exact value of $J_{nitrate}$ in the real atmosphere.

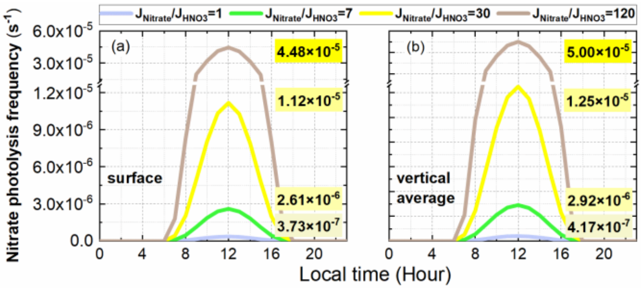

Figure 19 Diurnal patterns of surface-averaged (a) and vertically-averaged (b) simulations of the nitrate photolysis frequency with four different $J_{nitrate}/J_{HNO3}$ ratios (1, 7, 30, 120) at the 95 NCP sites during the study period (The nitrate photolysis frequencies at 12:00 are shown in each graph).

Table 4. Summary of studies on the nitrate photolysis frequency ($J_{nitrate}$) (J_{HNO3} denotes the photolysis frequency of gas HNO_3)

Experimental conditions	Main conclusion	Reference
HNO_3 absorbed on Pyrex surface	$J_{nitrate}$ (1.2×10^{-5} s^{-1}) is 1–2 orders of magnitude faster than in the gas and aqueous phases.	(Zhou et al., 2003)
Atmosphere simulation chamber	$J_{nitrate}$ on snow, ground, and glass surfaces, can be excluded in the chamber.	(Rohrer et al., 2005)
HNO_3 absorbed on glass surface	Photolysis frequency of surfaces adsorbed HNO_3 is > 2 orders of magnitude larger than J_{HNO3}.	(Zhu et al., 2008)
Urban grime-coated surface	$J_{nitrate}$ (1.2×10^{-3} s^{-1}) is 4 orders of magnitude faster than in water (10^{-7} s^{-1}).	(Baergen and Donaldson, 2013)
Various natural/artificial surfaces	$J_{nitrate}$ ranges from 6.0×10^{-6} s^{-1} to $3.7\times10^{-4}s^{-1}$, 1–3 orders of magnitude higher than J_{HNO3}	(Ye et al., 2016a)
Adsorbed HNO_3 on glass surfaces	Photolysis frequency of surfaces adsorbed HNO_3 (2.4×10^{-7} s^{-1}) is very low.	(Laufs and Kleffmann, 2016)

Aerosol filter samples	$J_{nitrate}$ ranges from 6.2×10^{-6} s^{-1} to 5.0×10^{-4} s^{-1} with a mean of 1.3×10^{-4} s^{-1}.	(Ye et al., 2017)
Nitrate aerosol in the MBL	$J_{nitrate}$ is ~10 times higher than J_{HNO3}.	(Reed et al., 2017)
$PM_{2.5}$ in Beijing	$J_{nitrate}$ (1.22×10^{-5} s^{-1} to 4.84×10^{-4} s^{-1}) is 1–3 orders of magnitude higher than J_{HNO3}.	(Bao et al., 2018)
Sea-salt particulate nitrate	$J_{nitrate}$ is 25–50 times higher than J_{HNO3}.	(Kasibhatla et al., 2018)
Particles collected on filters	$J_{nitrate}$ is ≤ 30 times J_{HNO3}.	(Romer et al., 2018)
CMAQ simulation	Nitrate photolysis contributed ~30% of noontime HONO with a $J_{nitrate}/J_{HNO3}$ ratio of ~120.	(Fu et al., 2019)
CMAQ simulation	A $J_{nitrate}/J_{HNO3}$ ratio of 100 better improved sulfate simulations than a $J_{nitrate}/J_{HNO3}$ ratio of 10.	(Zheng et al., 2020)
MCM Box model	Nitrate photolysis contribution to HONO was < 8% with a $J_{nitrate}/J_{HNO3}$ ratio of 30.	(Xue et al., 2020)
MCM Box model	Nitrate photolysis contributed ~40% of noontime HONO with a $J_{nitrate}/J_{HNO3}$ ratio of ~120.	(Shi et al., 2020)
Smog chamber	The $J_{nitrate}/J_{HNO3}$ ratio was <10 for suspended submicron $NaNO_3$ and NH_4NO_3.	(Shi et al., 2021)
CMAQ simulation	Nitrate photolysis contribution to surface HONO was ~1.0% with a $J_{nitrate}/J_{HNO3}$ ratio of 30.	(Zhang et al., 2021)
WRF-Chem simulation	The relative contribution of nitrate photolysis to HONO increased with rising altitude and nitrate photolysis contributed much larger in the ABL than near the surfaceto the enhanced O_3. On average, nitrate photolysis contributed ~5% of surface daytime HONO with a $J_{nitrate}/J_{HNO3}$ ratio of 30 (~1×10^{-5} s^{-1}) but contributed ~30–50% of the enhanced O_3 near the surface in NCP in hazy days.	This study

MBL: marine boundary layer; ABL: atmospheric boundary layer.

4.3 Interactions between heterogeneous HONO sources

Form the comparison of nitrate budget induced by the six potential HONO sources in **Fig.S3&S9**, we can find that Het_{ground} led to an significant increase in nitrate concentrations. In the real atmosphere, the NO_2 heterogeneous reactions and the $\mathrm{Phot_{nitrate}}$ reaction occur simultaneously, while the sensitivity tests only considered one specific HONO source for each case and neglected their interactions, leading to the underestimation of the $\mathrm{Phot_{nitrate}}$ impact to some extent. Take it into consideration, the $\mathrm{Phot_{nitrate}}$ impact on atmospheric oxidants and secondary pollutants would be even larger, especially during the haze aggravating process.

$\mathrm{Phot_{nitrate}}$ would in turn change NO_x concentrations to some extent. From the 95-site-averaged NO_2 concentrations shown in **Fig. 20**, we can find that $\mathrm{Phot_{nitrate}}$ slightly increased NO_2 concentrations in hazy days. The elevated NO_2 concentration could enhance HONO formation via the NO_2 heterogeneous reactions, nevertheless, due to the high background NO_2 concentrations in NCP (up to ~ 40 ppb at nighttime), the increment of NO_2 and the enhanced HONO formation from NO_2 caused by $\mathrm{Phot_{nitrate}}$ were small (<10%), but might have a larger impact on NO_x budgets in clean regions. From the above, a positive feedback relationship between the NO_2 heterogeneous reactions and the $\mathrm{Phot_{nitrate}}$ reaction could be found, these multi-processes worse the air quality during the haze aggravating processes.

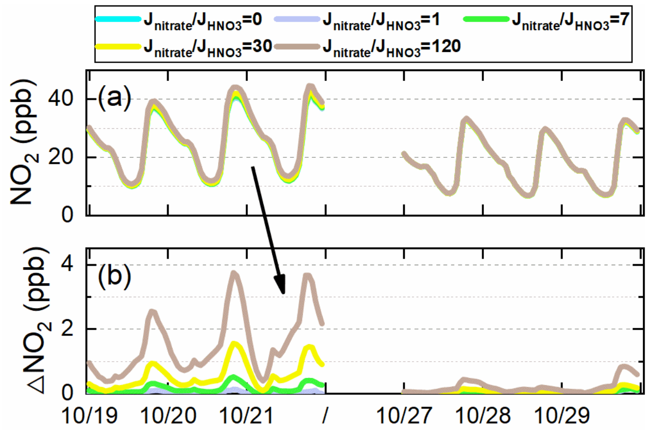

Figure 20 Comparison of 95-site-averaged simulations of NO_2 concentrations for the base case and four cases with different $J_{nitrate}/J_{HNO3}$ ratios (1, 7, 30 and 120) (a), and the corresponding NO_2 variations (b) compared with the base case in the North China Plain during Oct.11–31 of 2018.

5. Conclusions

In this study, three direct emission sources, the improved NO_2 heterogeneous reactions on aerosol and ground surfaces, and particulate nitrate photolysis in the atmosphere were included into the WRF-Chem model to explore the key HONO sources producing O_3 enhancements during typical autumn haze aggravating processes with co-occurrence of high $PM_{2.5}$ and O_3 in NCP. The six potential HONO sources produced a significant enhancement in surface HONO simulations and improved the mean HONO concentration at the BUCT site to 1.47 ppb from 0.05 ppb (improved the NMB to -14.22% from -97.11% and the IOA to 0.80 from 0.45). The improved HONO significantly enhanced the atmospheric oxidation capacity near the surface and at elevated heights, especially in hazy days, resulting in fast formation of and significant improvements of O_3 during haze aggravating processes in NCP. Although the photolysis frequency is usually lower during hazy days, higher concentrations of NO_2, $PM_{2.5}$ and nitrate favored HONO formation via heterogeneous reactions, leading to stronger atmospheric oxidation capacity. The major results include:

(1) For the surface HONO in NCP, Het_{ground} was the largest source during daytime and nighttime (~50–80%); the contribution of $Phot_{nitrate}$ ($J_{nitrate}/J_{HNO3} = 30$) to surface HONO concentrations was close to that of the NO+OH reaction during daytime (~1–12%) and was ~5% for daytime average; $E_{traffic}$ was important during nighttime (~10–20%) but small during daytime (<5%); the contribution of $Het_{aerosol}$ was minor (~2–3%) in daytime and <10% in nighttime; the contribution of E_{soil} was

<3%, and E_{indoor} could be neglected. Vertically, the HONO enhancements due to ground-based potential HONO sources ($E_{traffic}$, E_{soil}, E_{indoor} and Het_{ground}) decreased rapidly with height, while the NO+OH reaction and aerosol-related HONO sources ($Phot_{nitrate}$ and $Het_{aerosol}$) decreased with height much slower. The enhanced HONO due to $Phot_{nitrate}$ in hazy days was about ten times larger than in clean days and became the dominant HONO source (~30–70% when $J_{nitrate}/J_{HNO3} = 30$) at higher layers, and both HONO concentrations and $Phot_{nitrate}$ contributions increased with the aggravated pollution levels.

(2) Near the surface, daytime OH production/loss rates were significantly enhanced by~320% for the 6S case (mean was 5.27 ppb h^{-1}) compared with the base case (mean was 1.26 ppb h^{-1}); vertically, daytime OH production/loss rates were enhanced by ~105% for the 6S case (mean was 2.21 ppb h^{-1}) compared with the base case (mean was 1.08 ppb h^{-1}). The enhanced OH production rate and OH due to the six potential HONO sources both showed a strong positive correlation with $PM_{2.5}$ concentrations at the 95 NCP sites, with a slope of 0.043 ppb $h^{-1}/\mu g\ m^{-3}$ of $PM_{2.5}$ and 3.62×10^4 molec $cm^{-3}/\mu g\ m^{-3}$ of $PM_{2.5}$ from the surface to the height of 2.5 km for case 6S, respectively. The atmospheric oxidation capacity (e.g., OH) was enhanced in the haze aggravating process.

(3) A strong positive correlation (r>0.8) between enhanced O_3 by the six potential HONO sources and $PM_{2.5}$ concentrations was found in NCP, and nitrate photolysis was the largest contributor to the enhanced DMA8 O_3 in hazy days. Vertically, the enhanced DMA8 O_3 was < 2ppb when $PM_{2.5}$ was < 20μg m^{-3}, and that was >10 ppb

when $PM_{2.5}$ was > 60μg m^{-3} on average, with a slope of 0.24 ppb DMA8 O_3 enhancement /μg m^{-3} of $PM_{2.5}$. The surface enhanced DMA8 O_3 was ~5.5 ppb (Oct.19), ~7 ppb (Oct.20) and ~10 ppb (Oct.21), respectively, during a typical haze aggravating process, while that was usually ~2 ppb in clean days. The contribution of $Phot_{nitrate}$ to the enhanced DMA8 O_3 was increased by over one magnitude during the haze aggravating process (up to 5–10 ppb) compared with that in clean days (~0.1–0.5 ppb), reached ~2–4.5 ppb (Oct.19), ~3–6 ppb (Oct.20) and ~5–10 ppb (Oct.21), respectively, during a typical haze aggravating process vertically.

(4) Surface O_3 was controlled by VOCs-sensitive chemistry, while O_3 at higher altitude (>800m) was controlled by NO_x-sensitive chemistry in NCP during autumn. The nitrate photolysis reaction enhanced OH and NO_x concentrations, both favored O_3 formation at high altitude, especially in haze aggravating processes with abundant nitrate. The produced HONO rather than the produced NO_2 through nitrate photolysis had a stronger promotion for O_3 formation near the surface, but the impacts of the two products on O_3 enhancements were similar at higher altitude (~2000 m).

(5) Nitrate photolysis only contributed ~5% of the surface HONO in daytime with a $J_{nitrate}/J_{HNO3}$ ratio of 30 (~1×10^{-5} s^{-1}) but contributed ~30–50% of the enhanced O_3 near the surface in NCP in hazy days. The photolysis of nitrate had a limited impact on nitrate concentrations (reduced by <5% with $J_{nitrate}/J_{HNO3}$ =30, and <15% even with a $J_{nitrate}/J_{HNO3}$ ratio of 120), due mainly to the simultaneously enhanced atmospheric oxidants favoring the formation of HNO_3 and nitrate. Choosing a larger $J_{nitrate}$ value might cover up other ground-based unknown HONO sources, but

overestimate vertical sources of HONO, and NO_x and O_3 concentrations, so more studies are still needed to find the exact value of $J_{nitrate}$ in the real atmosphere.

Data availability

Data are available upon reasonable request to the corresponding authors.

Author contribution:

J.Z., C.L., J.A., M.G., and W.W. conceived and designed the research. J.Z. performed WRF-Chem simulations and wrote the paper. J.Z., C.L., Y.G., and H.R. performed data analyses and produced the figures. C.L., Y.Z., F.Z., X.F., C.Y., K.D., Y.L., and M.K. conducted the field observations. W.W., J.A., M.G., Y.L., and M.K. reviewed the article.

Competing interests

The authors declare that they have no conflict of interest.

Acknowledgements

This research was partially supported by the National Natural Science Foundation of China (Grant No. 92044302, 42075108, 42107124, 42075110, 41822703, 91544221, 91844301), Beijing National Laboratory for Molecular Sciences

(BNLMS-CXXM-202011) and the China Postdoctoral Science Foundation (grant NO. 2019M660764).

References

Alicke, B., Platt, U., Stutz, J., 2002. Impact of nitrous acid photolysis on the total hydroxyl radical budget during the Limitation of Oxidant Production/Pianura Padana Produzione di Ozono study in Milan. J Geophys Res-Atmos 107. doi:10.1029/2000JD000075.

An, J.L., Li, Y., Chen, Y., Li, J., Qu, Y., Tang, Y.J., 2013. Enhancements of major aerosol components due to additional HONO sources in the North China Plain and implications for visibility and haze. Advances in Atmospheric Sciences 30, 57-66.

Aumont, B., Chervier, F., Laval, S., 2003. Contribution of HONO sources to the $NO_x/HO_x/O_3$ chemistry in the polluted boundary layer. Atmospheric Environment 37, 487-498.

Avnery, S., Mauzerall, D.L., Liu, J., Horowitz, L.W., 2011a. Global crop yield reductions due to surface ozone exposure: 1. Year 2000 crop production losses and economic damage. Atmospheric Environment 45, 2284-2296.

Avnery, S., Mauzerall, D.L., Liu, J., Horowitz, L.W., 2011b. Global crop yield reductions due to surface ozone exposure: 2. Year 2030 potential crop production losses and economic damage under two scenarios of O_3 pollution. Atmospheric Environment 45, 2297-2309.

Baergen, A.M., Donaldson, D.J., 2013. Photochemical renoxification of nitric acid on real urban grime. Environmental Science & Technology 47, 815-820.

Bao, F., Li, M., Zhang, Y., Chen, C., Zhao, J., 2018. Photochemical Aging of Beijing Urban $PM_{2.5}$: HONO Production. Environmental Science & Technology 52, 6309-6316.

Bao, F.X., Jiang, H.Y., Zhang, Y., Li, M., Ye, C.X., Wang, W.G., Ge, M.F., Chen, C.C., Zhao, J.C., 2020. The Key Role of Sulfate in the Photochemical Renoxification on Real $PM_{2.5}$. Environmental Science & Technology 54, 3121-3128.

Bejan, I., Abd-el-Aal, Y., Barnes, I., Benter, T., Bohn, B., Wiesen, P., Kleffmann, J., 2006. The photolysis of ortho-nitrophenols: a new gas phase source of HONO. Physical chemistry chemical physics : PCCP 8, 2028-2035.

Chen, S., Wang, H., Lu, K., Zeng, L., Hu, M., Zhang, Y., 2020a. The trend of surface ozone in Beijing from 2013 to 2019: Indications of the persisting strong atmospheric oxidation capacity. Atmospheric Environment 242, 117801.

Chen, Y., Wang, W.G., Lian, C.F., Peng, C., Zhang, W.Y., Li, J.L., Liu, M.Y., Shi, B., Wang, X.F., Ge, M.F., 2020b. Evaluation and impact factors of indoor and outdoor gas-phase nitrous acid under different environmental conditions. Journal of Environmental Sciences 95, 165-171.

Chen, Y., Zheng, P., Wang, Z., Pu, W., Tan, Y., Yu, C., Xia, M., Wang, W., Guo, J., Huang, D., Yan, C., Nie, W., Ling, Z., Chen, Q., Lee, S., Wang, T., 2021. Secondary Formation and Impacts of Gaseous Nitro-Phenolic Compounds in the Continental Outflow Observed at a Background Site in South China. Environmental Science & Technology. DOI: 10.1021/acs.est.1c04596.

Crowley, J.N., Carl, S.A., 1997. OH formation in the photoexcitation of NO2 beyond the dissociation threshold in the presence of water vapor. Journal of Physical Chemistry A 101, 4178-4184.

Cui, L., Li, R., Fu, H., Meng, Y., Zhao, Y., Li, Q., Chen, J., 2021. Nitrous acid emission from open burning of major crop residues in mainland China. Atmospheric Environment 244, 117950.

Dillon, T.J., Crowley, J.N., 2018. Reactive quenching of electronically excited NO_2^* and NO_3^* by H_2O as potential sources of atmospheric HO_x radicals. Atmospheric Chemistry and Physics 18, 14005-14015.

Dong, W., Xing, J., Wang, S., 2010. Temporal and spatial distribution of anthropogenic ammonia emissions in China: 1994-2006. Environmental Sciences (in Chinese) 31, 1457-1463.

Emmons, L.K., Walters, S., Hess, P.G., Lamarque, J.F., Pfister, G.G., Fillmore, D., Granier, C., Guenther, A., Kinnison, D., Laepple, T., Orlando, J., Tie, X., Tyndall, G., Wiedinmyer, C., Baughcum, S.L., Kloster, S., 2010. Description and evaluation of the Model for Ozone and Related chemical Tracers, version 4 (MOZART-4). Geoscientific Model Development 3, 43-67.

Feng, T., Zhao, S., Bei, N., Liu, S., Li, G., 2021. Increasing atmospheric oxidizing capacity weakens emission mitigation effort in Beijing during autumn haze events. Chemosphere 281, 130855.

Feng, Z., De Marco, A., Anav, A., Gualtieri, M., Sicard, P., Tian, H., Fornasier, F., Tao, F., Guo, A., Paoletti, E., 2019. Economic losses due to ozone impacts on human health, forest productivity and crop yield across China. Environ Int 131, 104966.

Feng, Z., Hu, E., Wang, X., Jiang, L., Liu, X., 2015. Ground-level O_3 pollution and its impacts on food crops in China: a review. Environ Pollut 199, 42-48.

Feng, Z., Xu, Y., Kobayashi, K., Dai, L., Zhang, T., Agathokleous, E., Calatayud, V., Paoletti, E., Mukherjee, A., Agrawal, M., Park, R.J., Oak, Y.J., Yue, X., 2022. Ozone pollution threatens the production of major staple crops in East Asia. Nature Food 3, 47-56.

Finlayson-Pitts, B.J., Wingen, L.M., Sumner, A.L., Syomin, D., Ramazan, K.A., 2003. The heterogeneous hydrolysis of NO_2 in laboratory systems and in outdoor and indoor atmospheres: An integrated mechanism. Physical Chemistry Chemical Physics 5, 223-242.

Fröhlich, R., Cubison, M.J., Slowik, J.G., Bukowiecki, N., Prévôt, A.S.H., Baltensperger, U., Schneider, J., Kimmel, J.R., Gonin, M., Rohner, U., Worsnop, D.R., Jayne, J.T., 2013. The ToF-ACSM: a portable aerosol chemical speciation monitor with TOFMS detection. Atmospheric Measurement Techniques 6, 3225-3241.

Fu, X., Wang, T., Gao, J., Wang, P., Liu, Y.M., Wang, S.X., Zhao, B., Xue, L.K., 2020. Persistent Heavy Winter Nitrate Pollution Driven by Increased Photochemical Oxidants in Northern China. Environmental Science & Technology 54, 3881-3889.

Fu, X., Wang, T., Zhang, L., Li, Q.Y., Wang, Z., Xia, M., Yun, H., Wang, W.H., Yu, C., Yue, D.L., Zhou, Y., Zheng, J.Y., Han, R., 2019. The significant contribution of HONO to secondary pollutants during a severe winter pollution event in southern China. Atmospheric Chemistry and Physics 19, 1-14.

Gao, W., Tan, G., Hong, Y., Li, M., Nian, H., Guo, C., Huang, Z., Fu, Z., Dong, J., Xu, X., 2013. Development of portable single photon ionization time-of-flight mass spectrometer combined with membrane inlet. International Journal of Mass Spectrometry 334, 8-12.

Ge, M., Tong, S., Wang, W., Zhang, W., Chen, M., Peng, C., Li, J., Zhou, L., Chen, Y., Liu, M., 2021. Important Oxidants and Their Impact on the Environmental Effects of Aerosols. The journal of physical chemistry. A.125, 3813-3825.

Ge, S., Wang, G., Zhang, S., Li, D., Xie, Y., Wu, C., Yuan, Q., Chen, J., Zhang, H., 2019. Abundant NH_3 in China Enhances Atmospheric HONO Production by Promoting the Heterogeneous Reaction of SO_2 with NO_2. Environmental Science & Technology 53, 14339-14347.

Gen, M., Liang, Z., Zhang, R., Go Mabato, B.R., Chan, C.K., 2022. Particulate nitrate photolysis in the atmosphere. Environmental Science: Atmospheres. DOI: 10.1039/D1EA00087J.

Gligorovski, S., Strekowski, R., Barbati, S., Vione, D., 2015. Environmental Implications of Hydroxyl Radicals (*OH). Chem Rev 115, 13051-13092.

Gómez Alvarez, E., Sörgel, M., Gligorovski, S., Bassil, S., Bartolomei, V., Coulomb, B., Zetzsch, C., Wortham, H., 2014. Light-induced nitrous acid (HONO) production from NO_2 heterogeneous reactions on household chemicals. Atmospheric Environment 95, 391-399.

Guenther, A.B., Jiang, X., Heald, C.L., Sakulyanontvittaya, T., Duhl, T., Emmons, L.K., Wang, X., 2012. The Model of Emissions of Gases and Aerosols from Nature version 2.1 (MEGAN2.1): an extended and updated framework for modeling biogenic emissions. Geoscientific Model Development 5, 1471-1492.

Guo, Y., Zhang, J., An, J., Qu, Y., Liu, X., Sun, Y., Chen, Y., 2020. Effect of vertical parameterization of a missing daytime source of HONO on concentrations of HONO, O_3 and secondary organic aerosols in eastern China. Atmospheric Environment 226, 117208.

Hendrick, F., Muller, J.F., Clemer, K., Wang, P., De Maziere, M., Fayt, C., Gielen, C., Hermans, C., Ma, J.Z., Pinardi, G., Stavrakou, T., Vlemmix, T., Van Roozendael, M., 2014. Four years of ground-based MAX-DOAS observations of HONO and NO_2 in the Beijing area. Atmospheric Chemistry and Physics 14, 765-781.

Huang, X., Li, M.M., Li, J.F., Song, Y., 2012. A high-resolution emission inventory of crop burning in fields in China based on MODIS Thermal Anomalies/Fire products. Atmospheric Environment 50, 9-15.

Kasibhatla, P., Sherwen, T., Evans, M.J., Carpenter, L.J., Reed, C., Alexander, B., Chen, Q.J., Sulprizio, M.P., Lee, J.D., Read, K.A., Bloss, W., Crilley, L.R., Keene, W.C., Pszenny, A.A.P., Hodzic, A., 2018. Global impact of nitrate photolysis in sea-salt aerosol on NO_x, OH, and O_3 in the marine boundary layer. Atmospheric Chemistry and Physics 18, 11185-11203.

Kim, S., VandenBoer, T.C., Young, C.J., Riedel, T.P., Thornton, J.A., Swarthout, B., Sive, B., Lerner, B., Gilman, J.B., Warneke, C., Roberts, J.M., Guenther, A., Wagner, N.L., Dube, W.P., Williams, E., Brown, S.S., 2014. The primary and recycling sources of OH during the NACHTT-2011 campaign: HONO as an important OH primary source in the wintertime. J Geophys Res-Atmos 119, 6886-6896.

Kleffmann, J., Kurtenbach, R., Lorzer, J., Wiesen, P., Kalthoff, N., Vogel, B., Vogel, H., 2003. Measured and simulated vertical profiles of nitrous acid - Part I: Field measurements. Atmospheric Environment 37, 2949-2955.

Klosterkother, A., Kurtenbach, R., Wiesen, P., Kleffmann, J., 2021. Determination of the emission indices for NO, NO_2, HONO, HCHO, CO, and particles emitted from candles. Indoor Air 31, 116-127.

Kramer, L.J., Crilley, L.R., Adams, T.J., Ball, S.M., Pope, F.D., Bloss, W.J., 2020. Nitrous acid (HONO) emissions under real-world driving conditions from vehicles in a UK road tunnel. Atmospheric Chemistry and Physics 20, 5231-5248.

Kubota, M., Asami, T., 1985. Volatilization of Nitrous-Acid from Upland Soils. Soil Science and Plant Nutrition 31, 27-34.

Kurtenbach, R., Becker, K.H., Gomes, J.A.G., Kleffmann, J., Lorzer, J.C., Spittler, M., Wiesen, P., Ackermann, R., Geyer, A., Platt, U., 2001. Investigations of emissions and heterogeneous formation of HONO in a road traffic tunnel. Atmospheric Environment 35, 3385-3394.

Laufs, S., Kleffmann, J., 2016. Investigations on HONO formation from photolysis of adsorbed HNO_3 on quartz glass surfaces. Physical Chemistry Chemical Physics 18, 9616-9625.

Lee, J.D., Whalley, L.K., Heard, D.E., Stone, D., Dunmore, R.E., Hamilton, J.F., Young, D.E., Allan, J.D., Laufs, S., Kleffmann, J., 2016. Detailed budget analysis of HONO in central London reveals a missing daytime source. Atmospheric Chemistry and Physics 16, 2747-2764.

Li, G., Lei, W., Zavala, M., Volkamer, R., Dusanter, S., Stevens, P., Molina, L.T., 2010. Impacts of HONO sources on the photochemistry in Mexico City during the MCMA-2006/MILAGO Campaign. Atmospheric Chemistry and Physics 10, 6551-6567.

Li, K., Jacob, D.J., Shen, L., Lu, X., De Smedt, I., Liao, H., 2020. Increases in surface ozone pollution in China from 2013 to 2019: anthropogenic and meteorological influences. Atmospheric Chemistry and Physics 20, 11423-11433.

Li, L., Chen, C.H., Huang, C., Huang, H.Y., Zhang, G.F., Wang, Y.J., Wang, H.L., Lou, S.R., Qiao, L.P., Zhou, M., Chen, M.H., Chen, Y.R., Streets, D.G., Fu, J.S., Jang, C.J., 2012. Process analysis of regional ozone formation over the Yangtze River Delta, China using the Community Multi-scale Air Quality modeling system. Atmospheric Chemistry and Physics 12, 10971-10987.

Li, M., Zhang, Q., Kurokawa, J., Woo, J.H., He, K.B., Lu, Z.F., Ohara, T., Song, Y., Streets, D.G., Carmichael, G.R., Cheng, Y.F., Hong, C.P., Huo, H., Jiang, X.J., Kang, S.C., Liu, F., Su, H., Zheng, B., 2017. MIX: a mosaic Asian anthropogenic emission inventory under the international collaboration framework of the MICS-Asia and HTAP. Atmospheric Chemistry and Physics 17, 935-963.

Li, S., Matthews, J., Sinha, A., 2008. Atmospheric hydroxyl radical production from electronically excited NO_2 and H_2O. Science 319, 1657-1660.

Li, X., Rohrer, F., Hofzumahaus, A., Brauers, T., Häseler, R., Bohn, B., Broch, S., Fuchs, H., Gomm, S., Holland, F., 2015. Response to Comment on "Missing gas-phase source of HONO inferred from Zeppelin measurements in the troposphere". Science 348, 1326-1326.

Li, X., Rohrer, F., Hofzumahaus, A., Brauers, T., Haseler, R., Bohn, B., Broch, S., Fuchs, H., Gomm, S., Holland, F., Jager, J., Kaiser, J., Keutsch, F.N., Lohse, I., Lu, K., Tillmann, R., Wegener, R., Wolfe, G.M., Mentel, T.F., Kiendler-Scharr, A., Wahner, A., 2014. Missing gas-phase source of HONO inferred from Zeppelin measurements in the troposphere. Science 344, 292-296.

Li, Y., An, J.L., Min, M., Zhang, W., Wang, F., Xie, P.H., 2011. Impacts of HONO sources on the air quality in Beijing, Tianjin and Hebei Province of China. Atmospheric Environment 45, 4735-4744.

Liao, S., Zhang, J., Yu, F., Zhu, M., Liu, J., Ou, J., Dong, H., Sha, Q., Zhong, Z., Xie, Y., Luo, H., Zhang, L., Zheng, J., 2021. High Gaseous Nitrous Acid (HONO) Emissions from Light-Duty Diesel Vehicles. Environmental science & technology 55, 200-208.

Lin, Y.L., Farley, R.D., Orville, H.D., 1983. Bulk Parameterization of the Snow Field in a Cloud Model. J Clim Appl Meteorol 22, 1065-1092.

Liu, J., Li, S., Zeng, J., Mekic, M., Yu, Z., Zhou, W., Loisel, G., Gandolfo, A., Song, W., Wang, X., Zhou, Z., Herrmann, H., Li, X., Gligorovski, S., 2019. Assessing indoor gas phase oxidation capacity through real-time measurements of HONO and NO_x in Guangzhou, China. Environ Sci Process Impacts 21, 1393-1402.

Liu, Y., Zhang, Y., Lian, C., Yan, C., Feng, Z., Zheng, F., Fan, X., Chen, Y., Wang, W., Chu, B., Wang, Y., Cai, J., Du, W., Daellenbach, K.R., Kangasluoma, J., Bianchi, F., Kujansuu, J., Petäjä, T., Wang, X., Hu, B., Wang, Y., Ge, M., He, H., Kulmala, M., 2020. The promotion effect of nitrous acid on aerosol formation in wintertime in Beijing: the possible contribution of traffic-related emissions. Atmospheric Chemistry and Physics 20, 13023-13040.

Liu, Z., Wang, Y., Costabile, F., Amoroso, A., Zhao, C., Huey, L.G., Stickel, R., Liao, J., Zhu, T., 2014. Evidence of aerosols as a media for rapid daytime HONO production over China. Environmental Science & Technology 48, 14386-14391.

Lu, X., Zhang, L., Wang, X.L., Gao, M., Li, K., Zhang, Y.Z., Yue, X., Zhang, Y.H., 2020. Rapid Increases in Warm-Season Surface Ozone and Resulting Health Impact in China Since 2013. Environmental Science & Technology Letters 7, 240-247.

Ma, J., Liu, Y., Han, C., Ma, Q., Liu, C., He, H., 2013. Review of heterogeneous photochemical reactions of NO_y on aerosol — A possible daytime source of nitrous acid (HONO) in the atmosphere. Journal of Environmental Sciences 25, 326-334.

Ma, Z.Q., Xu, J., Quan, W.J., Zhang, Z.Y., Lin, W.L., Xu, X.B., 2016. Significant increase of surface ozone at a rural site, north of eastern China. Atmospheric Chemistry and Physics 16, 3969-3977.

Maji, K.J., Namdeo, A., 2021. Continuous increases of surface ozone and associated premature mortality growth in China during 2015-2019. Environ Pollut 269, 116183.

Marion, A., Morin, J., Gandolfo, A., Ormeno, E., D'Anna, B., Wortham, H., 2021. Nitrous acid formation on Zea mays leaves by heterogeneous reaction of nitrogen dioxide in the laboratory. Environ Res 193, 110543.

Meng, F.H., Qin, M., Tang, K., Duan, J., Fang, W., Liang, S.X., Ye, K.D., Xie, P.H., Sun, Y.L., Xie, C.H., Ye, C.X., Fu, P.Q., Liu, J.G., Liu, W.Q., 2020. High-resolution vertical distribution and sources of HONO and NO_2 in the nocturnal boundary layer in urban Beijing, China. Atmospheric Chemistry and Physics 20, 5071-5092.

Mills, G., Buse, A., Gimeno, B., Bermejo, V., Holland, M., Emberson, L., Pleijel, H., 2007. A synthesis of AOT40-based response functions and critical levels of ozone for agricultural and horticultural crops. Atmospheric Environment 41, 2630-2643.

Mills, G., Sharps, K., Simpson, D., Pleijel, H., Broberg, M., Uddling, J., Jaramillo, F., Davies, W.J., Dentener, F., Van den Berg, M., Agrawal, M., Agrawal, S.B., Ainsworth, E.A., Buker, P., Emberson, L., Feng, Z., Harmens, H., Hayes, F., Kobayashi, K., Paoletti, E., Van Dingenen, R., 2018. Ozone pollution will compromise efforts to increase global wheat production. Glob Chang Biol 24, 3560-3574.

Oswald, R., Behrendt, T., Ermel, M., Wu, D., Su, H., Cheng, Y., Breuninger, C., Moravek, A., Mougin, E., Delon, C., Loubet, B., Pommerening-Roser, A., Sorgel, M., Poschl, U., Hoffmann, T., Andreae, M.O., Meixner, F.X., Trebs, I., 2013. HONO emissions from soil bacteria as a major source of atmospheric reactive nitrogen. Science 341, 1233-1235.

Pagsberg, P., Bjergbakke, E., Ratajczak, E., Sillesen, A., 1997. Kinetics of the gas phase reaction OH+NO (+M)->HONO (+M) and the determination of the UV absorption cross sections of HONO. Chemical Physics Letters 272, 383-390.

Perner, D., Platt, U., 1979. Detection of nitrous acid in the atmospeere by differential optical absorption. Geophysical Research Letters 6, 917-920.

Pitts, J.N., Wallington, T.J., Biermann, H.W., Winer, A.M., 1985. Identification and Measurement of Nitrous-Acid in an Indoor Environment. Atmospheric Environment 19, 763-767.

Qu, Y., Chen, Y., Liu, X., Zhang, J., Guo, Y., An, J., 2019. Seasonal effects of additional HONO sources and the heterogeneous reactions of N_2O_5 on nitrate in the North China Plain. The Science of the total environment 690, 97-107.

Reed, C., Evans, M.J., Crilley, L.R., Bloss, W.J., Sherwen, T., Read, K.A., Lee, J.D., Carpenter, L.J., 2017. Evidence for renoxification in the tropical marine boundary layer. Atmospheric Chemistry and Physics 17, 4081-4092.

Richards, B.L., Middleton, J.T., Hewitt, W.B., 1958. Air Pollution With Relation to Agronomic Crops: V. Oxidant Stipple of Grape. Agronomy Journal 50, 559-561.

Rohrer, F., Bohn, B., Brauers, T., Bruning, D., Johnen, F.J., Wahner, A., Kleffmann, J., 2005. Characterisation of the photolytic HONO-source in the atmosphere simulation chamber SAPHIR. Atmospheric Chemistry and Physics 5, 2189-2201.

Romer, P.S., Wooldridge, P.J., Crounse, J.D., Kim, M.J., Wennberg, P.O., Dibb, J.E., Scheuer, E., Blake, D.R., Meinardi, S., Brosius, A.L., Thames, A.B., Miller, D.O., Brune, W.H., Hall, S.R., Ryerson, T.B., Cohen, R.C., 2018. Constraints on Aerosol Nitrate Photolysis as a Potential Source of HONO and NO_x. Environmental Science & Technology 52, 13738-13746.

Rondon, A., Sanhueza, E., 1989. High HONO atmospheric concentrations during vegetation burning in the tropical savannah. Tellus Ser. B-Chem. Phys. Meteorol. 41, 474-477.

Ryan, R.G., Rhodes, S., Tully, M., Wilson, S., Jones, N., Friess, U., Schofield, R., 2018. Daytime HONO, NO_2 and aerosol distributions from MAX-DOAS observations in Melbourne. Atmospheric Chemistry and Physics 18, 13969-13985.

Saliba, N.A., Mochida, M., Finlayson-Pitts, B.J., 2000. Laboratory studies of sources of HONO in polluted urban atmospheres. Geophysical Research Letters 27, 3229-3232.

Sakamaki, F., Hatakeyama, S., Akimoto, H., 1983. Formation of Nitrous-Acid and Nitric-Oxide in the Heterogeneous Dark Reaction of Nitrogen-Dioxide and Water-Vapor in a Smog Chamber. International Journal of Chemical Kinetics 15, 1013-1029.

Sarwar, G., Roselle, S.J., Mathur, R., Appel, W., Dennis, R.L., Vogel, B., 2008. A comparison of CMAQ HONO predictions with observations from the northeast oxidant and particle study. Atmospheric Environment 42, 5760-5770.

Selin, N.E., Wu, S., Nam, K.M., Reilly, J.M., Paltsev, S., Prinn, R.G., Webster, M.D., 2009. Global health and economic impacts of future ozone pollution. Environmental Research Letters 4, 044014.

Shi, Q., Tao, Y., Krechmer, J.E., Heald, C.L., Murphy, J.G., Kroll, J.H., Ye, Q., 2021. Laboratory Investigation of Renoxification from the Photolysis of Inorganic Particulate Nitrate. Environmental science & technology, 55, 854−861.

Shi, X., Ge, Y., Zheng, J., Ma, Y., Ren, X., Zhang, Y., 2020. Budget of nitrous acid and its impacts on atmospheric oxidative capacity at an urban site in the central Yangtze River Delta region of China. Atmospheric Environment 238, 117725.

Sillman, S., 1995. The use of NO_y , H_2O_2, and HNO_3 as indicators for ozone-NO_x-hydrocarbon sensitivity in urban locations. Journal of Geophysical Research: Atmospheres 100, 14175-14188.

Slater, E.J., Whalley, L.K., Woodward-Massey, R., Ye, C.X., Lee, J.D., Squires, F., Hopkins, J.R., Dunmore, R.E., Shaw, M., Hamilton, J.F., Lewis, A.C., Crilley, L.R., Kramer, L., Bloss, W., Vu, T., Sun, Y.L., Xu, W.Q., Yue, S.Y., Ren, L.J., Acton, W.J.F., Hewitt, C.N., Wang, X.M., Fu, P.Q., Heard, D.E., 2020. Elevated levels of OH observed in haze events during wintertime in central Beijing. Atmospheric Chemistry and Physics 20, 14847-14871.

Sorgel, M., Trebs, I., Serafimovich, A., Moravek, A., Held, A., Zetzsch, C., 2011. Simultaneous HONO measurements in and above a forest canopy: influence of turbulent exchange on mixing ratio differences. Atmospheric Chemistry and Physics 11, 841-855.

Stuhl, F., Niki, H., 1972. Flash Photochemical Study of the Reaction OH+NO+M Using Resonance Fluorescent Detection of OH. The Journal of Chemical Physics 57, 3677-3679.

Tan, Z.F., Rohrer, F., Lu, K.D., Ma, X.F., Bohn, B., Broch, S., Dong, H.B., Fuchs, H., Gkatzelis, G.I., Hofzumahaus, A., Holland, F., Li, X., Liu, Y., Liu, Y.H., Novelli, A., Shao, M., Wang, H.C., Wu, Y.S., Zeng, L.M., Hu, M., Kiendler-Scharr, A., Wahner, A., Zhang, Y.H., 2018. Wintertime photochemistry in Beijing: observations of RO_x radical concentrations in the North China Plain during the BEST-ONE campaign. Atmospheric Chemistry and Physics 18, 12391-12411.

Tang, M.J., Huang, X., Lu, K.D., Ge, M.F., Li, Y.J., Cheng, P., Zhu, T., Ding, A.J., Zhang, Y.H., Gligorovski, S., Song, W., Ding, X., Bi, X.H., Wang, X.M., 2017. Heterogeneous reactions of mineral dust aerosol: implications for tropospheric oxidation capacity. Atmospheric Chemistry and Physics 17, 11727-11777.

Tang, Y., An, J., Wang, F., Li, Y., Qu, Y., Chen, Y., Lin, J., 2015. Impacts of an unknown daytime HONO source on the mixing ratio and budget of HONO, and hydroxyl, hydroperoxyl, and organic peroxy radicals, in the coastal regions of China. Atmospheric Chemistry and Physics 15, 9381-9398.

Theys, N., Volkamer, R., Mueller, J.F., Zarzana, K.J., Kille, N., Clarisse, L., De Smedt, I., Lerot, C., Finkenzeller, H., Hendrick, F., Koenig, T.K., Lee, C.F., Knote, C., Yu, H., Van Roozendael, M., 2020. Global nitrous acid emissions and levels of regional oxidants enhanced by wildfires. Nature Geoscience 13, 681-686.

Tie, X., Long, X., Li, G., Zhao, S., Cao, J., Xu, J., 2019. Ozone enhancement due to the photodissociation of nitrous acid in eastern China. Atmospheric Chemistry and Physics 19, 11267-11278.

VandenBoer, T.C., Brown, S.S., Murphy, J.G., Keene, W.C., Young, C.J., Pszenny, A.A.P., Kim, S., Warneke, C., de Gouw, J.A., Maben, J.R., Wagner, N.L., Riedel, T.P., Thornton, J.A., Wolfe, D.E., Dube, W.P., Ozturk, F., Brock, C.A., Grossberg, N., Lefer, B., Lerner, B., Middlebrook, A.M., Roberts, J.M., 2013. Understanding the role of the ground surface in HONO vertical structure: High resolution vertical profiles during NACHTT-11. J Geophys Res-Atmos 118, 10155-10171.

Villena, G., Kleffmann, J., Kurtenbach, R., Wiesen, P., Lissi, E., Rubio, M.A., Croxatto, G., Rappenglück, B., 2011. Vertical gradients of HONO, NO_x and O_3 in Santiago de Chile. Atmospheric Environment 45, 3867-3873.

Wang, F., An, J.L., Li, Y., Tang, Y.J., Lin, J., Qu, Y., Chen, Y., Zhang, B., Zhai, J., 2014. Impacts of uncertainty in AVOC emissions on the summer RO_x budget and ozone production rate in the three most rapidly-developing economic growth regions of China. Advances in Atmospheric Sciences 31, 1331-1342.

Wang, X., Zhang, Y., Hu, Y., Zhou, W., Lu, K., Zhong, L., Zeng, L., Shao, M., Hu, M., Russell, A.G., 2010. Process analysis and sensitivity study of regional ozone formation over the Pearl River Delta, China, during the PRIDE-PRD2004 campaign using the Community Multiscale Air Quality modeling system. Atmospheric Chemistry and Physics 10, 4423-4437.

Wang, Y., Apituley, A., Bais, A., Beirle, S., Benavent, N., Borovski, A., Bruchkouski, I., Chan, K.L., Donner, S., Drosoglou, T., Finkenzeller, H., Friedrich, M.M., Friess, U., Garcia-Nieto, D., Gomez-Martin, L., Hendrick, F., Hilboll, A., Jin, J.L., Johnston, P., Koenig, T.K., Kreher, K., Kumar, V., Kyuberis, A., Lampel, J., Liu, C., Liu, H.R., Ma, J.Z., Polyansky, O.L., Postylyakov, O., Querel, R., Saiz-Lopez, A., Schmitt, S., Tian, X., Tirpitz, J.L., Van Roozendael, M., Volkamer, R., Wang, Z.R., Xie, P.H., Xing, C.Z., Xu, J., Yela, M., Zhang, C.X., Wagner, T., 2020. Inter-comparison of MAX-DOAS measurements of tropospheric HONO slant column densities and vertical profiles during the CINDI-2 campaign. Atmospheric Measurement Techniques 13, 5087-5116.

Wang, Y., Dörner, S., Donner, S., Böhnke, S., De Smedt, I., Dickerson, R.R., Dong, Z., He, H., Li, Z., Li, Z., Li, D., Liu, D., Ren, X., Theys, N., Wang, Y., Wang, Y., Wang, Z., Xu, H., Xu, J., Wagner, T., 2019. Vertical profiles of NO_2, SO_2, HONO, HCHO, CHOCHO and aerosols derived from MAX-DOAS measurements at a rural site in the central western North China Plain and their relation to emission sources and effects of regional transport. Atmospheric Chemistry and Physics 19, 5417-5449.

Wilkinson, S., Mills, G., Illidge, R., Davies, W.J., 2012. How is ozone pollution reducing our food supply? J Exp Bot 63, 527-536.

Wong, K.W., Oh, H.J., Lefer, B.L., Rappengluck, B., Stutz, J., 2011. Vertical profiles of nitrous acid in the nocturnal urban atmosphere of Houston, TX. Atmospheric Chemistry and Physics 11, 3595-3609.

Wong, K.W., Tsai, C., Lefer, B., Haman, C., Grossberg, N., Brune, W.H., Ren, X., Luke, W., Stutz, J., 2012. Daytime HONO vertical gradients during SHARP 2009 in Houston, TX. Atmospheric Chemistry and Physics 12, 635-652.

Wu, D., Horn, M.A., Behrendt, T., Muller, S., Li, J., Cole, J.A., Xie, B., Ju, X., Li, G., Ermel, M., Oswald, R., Frohlich-Nowoisky, J., Hoor, P., Hu, C., Liu, M., Andreae, M.O., Poschl, U., Cheng, Y., Su, H., Trebs, I., Weber, B., Sorgel, M., 2019. Soil HONO emissions at high moisture content are driven by microbial nitrate reduction to nitrite: tackling the HONO puzzle. ISME J 13, 1688-1699.

Xing, C., Liu, C., Hu, Q., Fu, Q., Wang, S., Lin, H., Zhu, Y., Wang, S., Wang, W., Javed, Z., 2021. Vertical distributions of wintertime atmospheric nitrogenous compounds and the corresponding OH radicals production in Leshan, southwest China. Journal of Environmental Sciences 105, 44-55.

Xing, L., Wu, J.R., Elser, M., Tong, S.R., Liu, S.X., Li, X., Liu, L., Cao, J.J., Zhou, J.M., El-Haddad, I., Huang, R.J., Ge, M.F., Tie, X.X., Prevot, A.S.H., Li, G.H., 2019. Wintertime secondary organic aerosol formation in Beijing-Tianjin-Hebei (BTH): contributions of HONO sources and heterogeneous reactions. Atmospheric Chemistry and Physics 19, 2343-2359.

Xu, J., Zhang, Y.H., Wang, W., 2006. Numerical study on the impacts of heterogeneous reactions on ozone formation in the Beijing urban area. Advances in Atmospheric Sciences 23, 605-614.

Xu, W., Yang, W., Han, C., Yang, H., Xue, X., 2021. Significant influences of TiO_2 crystal structures on NO_2 and HONO emissions from the nitrates photolysis. Journal of Environmental Sciences 102, 198-206.

Xue, C., Zhang, C., Ye, C., Liu, P., Catoire, V., Krysztofiak, G., Chen, H., Ren, Y., Zhao, X., Wang, J., Zhang, F., Zhang, C., Zhang, J., An, J., Wang, T., Chen, J., Kleffmann, J., Mellouki, A., Mu, Y., 2020. HONO Budget and Its Role in Nitrate Formation in the Rural North China Plain. Environmental Science & Technology 54, 11048-11057.

Xue, C.Y., Ye, C., Zhang, C.L., Catoire, V., Liu, P.F., Gu, R.R., Zhang, J.W., Ma, Z.B., Zhao, X.X., Zhang, W.Q., Ren, Y.G., Krysztofiak, G., Tong, S.R., Xue, L.K., An, J.L., Ge, M.F., Mellouki, A., Mu, Y.J., 2021. Evidence for Strong HONO Emission from Fertilized Agricultural Fields and its Remarkable Impact on Regional O_3 Pollution in the Summer North China Plain. ACS Earth Space Chem. 5, 340-347.

Yang, K., Kong, L., Tong, S., Shen, J., Chen, L., Jin, S., Wang, C., Sha, F., Wang, L., 2021a. Double High-Level Ozone and $PM_{2.5}$ Co-Pollution Episodes in Shanghai, China: Pollution Characteristics and Significant Role of Daytime HONO. Atmosphere 12, 557.

Yang, W., Han, C., Yang, H., Xue, X., 2018. Significant HONO formation by the photolysis of nitrates in the presence of humic acids. Environ Pollut 243, 679-686.

Yang, W., Han, C., Zhang, T., Tang, N., Yang, H., Xue, X., 2021b. Heterogeneous photochemical uptake of NO_2 on the soil surface as an important ground-level HONO source. Environ. Pollut. 271, 116289.

Ye, C., Gao, H., Zhang, N., Zhou, X., 2016a. Photolysis of Nitric Acid and Nitrate on Natural and Artificial Surfaces. Environmental Science & Technology 50, 3530-3536.

Ye, C., Zhang, N., Gao, H., Zhou, X., 2017. Photolysis of Particulate Nitrate as a Source of HONO and NO_x. Environmental Science & Technology 51, 6849-6856.

Ye, C., Zhou, X., Pu, D., Stutz, J., Festa, J., Spolaor, M., Cantrell, C., Mauldin, R.L., Weinheimer, A., Haggerty, J., 2015. Comment on "Missing gas-phase source of HONO inferred from Zeppelin measurements in the troposphere". Science 348, 1326-d.

Ye, C., Zhou, X., Pu, D., Stutz, J., Festa, J., Spolaor, M., Tsai, C., Cantrell, C., Mauldin, R.L., 3rd, Campos, T., Weinheimer, A., Hornbrook, R.S., Apel, E.C., Guenther, A., Kaser, L., Yuan, B., Karl, T., Haggerty, J., Hall, S., Ullmann, K., Smith, J.N., Ortega, J., Knote, C., 2016b. Rapid cycling of reactive nitrogen in the marine boundary layer. Nature 532, 489-491.

Zaveri, R.A., Easter, R.C., Fast, J.D., Peters, L.K., 2008. Model for Simulating Aerosol Interactions and Chemistry (MOSAIC). J Geophys Res-Atmos 113. doi:10.1029/2007JD008782.

Zhang, H.L., Li, J.Y., Ying, Q., Yu, J.Z., Wu, D., Cheng, Y., He, K.B., Jiang, J.K., 2012. Source apportionment of $PM_{2.5}$ nitrate and sulfate in China using a source-oriented chemical transport model. Atmospheric Environment 62, 228-242.

Zhang, J., An, J., Qu, Y., Liu, X., Chen, Y., 2019a. Impacts of potential HONO sources on the concentrations of oxidants and secondary organic aerosols in the Beijing-Tianjin-Hebei region of China. The Science of the total environment 647, 836-852.

Zhang, J., Chen, J., Xue, C., Chen, H., Zhang, Q., Liu, X., Mu, Y., Guo, Y., Wang, D., Chen, Y., Li, J., Qu, Y., An, J., 2019b. Impacts of six potential HONO sources on HO_x budgets and SOA formation during a wintertime heavy haze period in the North China Plain. The Science of the total environment 681, 110-123.

Zhang, J., Guo, Y., Qu, Y., Chen, Y., Yu, R., Xue, C., Yang, R., Zhang, Q., Liu, X., Mu, Y., Wang, J., Ye, C., Zhao, H., Sun, Q., Wang, Z., An, J., 2020a. Effect of potential HONO sources on peroxyacetyl nitrate (PAN) formation in eastern China in winter. Journal of Environmental Sciences 94, 81-87.

Zhang, J., Ran, H., Guo, Y., Xue, C., Liu, X., Qu, Y., Sun, Y., Zhang, Q., Mu, Y., Chen, Y., Wang, J., An, J., 2022. High crop yield losses induced by potential HONO sources — A modelling study in the North China Plain. Science of The Total Environment 803, 149929.

Zhang, L., Wang, T., Zhang, Q., Zheng, J.Y., Xu, Z., Lv, M.Y., 2016. Potential sources of nitrous acid (HONO) and their impacts on ozone: A WRF-Chem study in a polluted subtropical region. J Geophys Res-Atmos 121, 3645-3662.

Zhang, N., Zhou, X.L., Shepson, P.B., Gao, H.L., Alaghmand, M., Stirm, B., 2009. Aircraft measurement of HONO vertical profiles over a forested region. Geophysical Research Letters 36. doi:10.1029/2009GL038999.

Zhang, Q., Geng, G., 2019. Impact of clean air action on $PM_{2.5}$ pollution in China. Science China Earth Sciences 62, 1845-1846.

Zhang, S., Sarwar, G., Xing, J., Chu, B., Xue, C., Sarav, A., Ding, D., Zheng, H., Mu, Y., Duan, F., Ma, T., He, H., 2021. Improving the representation of HONO chemistry in CMAQ and examining its impact on haze over China. Atmospheric Chemistry and Physics 21, 15809-15826.

Zhang, W., Tong, S., Ge, M., An, J., Shi, Z., Hou, S., Xia, K., Qu, Y., Zhang, H., Chu, B., Sun, Y., He, H., 2019c. Variations and sources of nitrous acid (HONO) during a severe pollution episode in Beijing in winter 2016. The Science of the total environment 648, 253-262.

Zhang, W.Q., Tong, S.R., Jia, C.H., Wang, L.L., Liu, B.X., Tang, G.Q., Ji, D.S., Hu, B., Liu, Z.R., Li, W.R., Wang, Z., Liu, Y., Wang, Y.S., Ge, M.F., 2020b. Different HONO Sources for Three Layers at the Urban Area of Beijing. Environmental science & technology 54, 12870-12880.

Zhao, H., Zhang, Y., Qi, Q., Zhang, H., 2021. Evaluating the Impacts of Ground-Level O_3 on Crops in China. Current Pollution Reports 7, 565-578.

Zheng, H., Song, S., Sarwar, G., Gen, M., Wang, S., Ding, D., Chang, X., Zhang, S., Xing, J., Sun, Y., Ji, D., Chan, C.K., Gao, J., McElroy, M.B., 2020. Contribution of Particulate Nitrate Photolysis to Heterogeneous Sulfate Formation for Winter Haze in China. Environmental Science & Technology Letters 7, 632-638.

Zhou, X., Gao, H., He, Y., Huang, G., Bertman, S.B., Civerolo, K., Schwab, J., 2003. Nitric acid photolysis on surfaces in low-NO_x environments: Significant atmospheric implications. Geophysical Research Letters 30. doi:10.1029/2003GL018620.

Zhu, C., Xiang, B., Zhu, L., Cole, R., 2008. Determination of absorption cross sections of surface-adsorbed HNO_3 in the 290–330 nm region by Brewster angle cavity ring-down spectroscopy. Chemical Physics Letters 458, 373-377.

Zhu, Y.W., Liu, W.Q., Fang, J., Xie, P.H., Dou, K., Qin, M., Si, F.Q., 2011. Monitoring and Analysis of Vertical Profile of Atmospheric HONO, NO_2 in Boundary Layer of Beijing. Spectroscopy and Spectral Analysis 31, 1078-1082.